Geophysical Characterisation and Monitoring of Earth Embankment Dams

Richard Cottrell BSc MSc FGS

MSc by Research

Swansea University
Prifysgol Abertawe

Declarations

This work has not previously been accepted in substance for any degree and is not being concurrently submitted in candidature for any degree.

Signed: [redacted]

Date: 31/03/2023

This thesis is the result of my own investigations, except where otherwise stated. Other sources are acknowledged by footnotes giving explicit references. A bibliography is appended.

Signed: [redacted]

Date: 31/03/2023

I hereby give consent for my thesis, if accepted, to be available for photocopying and for inter-library loans after expiry of a bar on access approved by the University.

Signed: [redacted]

Date: 31/03/2023

The University's ethical procedures have been followed and, where appropriate, that ethical approval has been granted.

Signed: [redacted]

Date: 31/03/2023

Acknowledgements

I would like to thank the following people and organisations, without whom I would not have been able to complete this MSc by Research:

KESS 2 East, the European Social Fund, Swansea University, and TerraDat UK Ltd. for funding this project and providing the support need to complete this research. I would like to thank the staff of Swansea University and the KESS 2 East office ensuring the smooth administrative operation of the project. I would also like to thank Ed Pritchard from Dŵr Cymru Welsh Water for providing a study site and essential information pertaining to it.

I would like the thank Professor Bernd Kulessa and Professor Tavi Murray for their support and contribution as my First and Second Supervisors, respectively. Through sharing their knowledge and experience of the world of environmental geophysics and academia, I have gained a newfound appreciation for these two worlds and the role they must play in environmental science.

I would also like thank Dr Joanna Hamlyn as my Company Supervisor for her help and support throughout this project. I would like to also extend my thanks to the rest of the TerraDat UK Ltd. team, in particular Dr Rob McDonald and Christian Bird for their support throughout this MSC and my previous MSc at Cardiff University. I have worked for and conducted research for TerraDat UK Ltd. since May 2020, and I am extremely grateful for the experiences they have made available to me. Through working and conducting research, I have gained a valuable insight into the world of geophysics and the world of ground engineering.

I would like to thank my family and friends for their support throughout this project. This research was conducted under the presidents of the COVID 19 Pandemic. At times it was difficult to find the continued motivation to complete with this project and without their support this would have been neigh-on impossible. Thank you.

Abstract

Geophysics has become fundamental in characterising earth embankment dams and identifying preferential seepage pathways, problem areas, and structural defects. The issue of non-uniqueness is profound in the interpretation of geophysical data, with features often attributed to multiple potential sources. This project tackles this issue by applying a multidisciplinary approach comprising traditional techniques to a study site in South Wales. These techniques comprised ground conductivity, magnetometry, and Electrical Resistivity Tomography (ERT). The computation of normalised chargeability data from an Induced Polarisation (IP) survey, normally used for mineral exploration, was applied to delineate between clay and moisture rich areas. This eliminated the issue of non-uniqueness between these two subsurface conditions. The application of these techniques led to successful characterisation of the embankment in terms of its engineered and natural components and identified a potential seepage pathway attributed to surface waters.

The Self-Potential (SP) method was evolved into a monitoring solution, building on the research and development of TerraDat Ltd's SPiVolt system. A methodology was developed to efficiently fabricate and install an SP monitoring network. SP monitoring confirmed the presence of the preferential seepage pathway hypothesised through the characterisation survey and identified a second pathway through the dam's core.

Dŵr Cymru Welsh Water have since used the results of this project to design a targeted grouting campaign and install surface drainage at the site. Comprehensive understanding of the material composition and temporal variations of subsurface conditions is considered essential for ensuring dam and reservoir owners achieve their aims of climate resilience and asset protection. The geophysical characterisation and monitoring methodology presented in this thesis provides an effective low-cost solution that can be applied to multiple scenarios such as landslide investigations, coal tip stability assessments and other hydrogeological problems.
.

Contents

1 Introduction

1.1 Earth Embankment Dam Characterisation and Monitoring Requisite

Accurate information about earth embankment bodies, foundations, geology, and their impounded reservoirs is required for safe operation. Different characterisation and monitoring techniques can be applied to the investigation, design, construction, and operation of earth embankment dams. When selecting or developing characterisation and monitoring methods, it is important to consider the following:

1. The suitability of a method: its accuracy and precision.
2. The ease of operation: how easy the method is to implement and acquire reliable data.
3. Durability: how well the method can cope with adverse weather conditions and being tampered with.
4. Repair and replacement: accessibility of the method and its maintenance costs.

Through the characterisation and monitoring of earth embankment dams, dam safety can be assessed and unveil helpful information that can be used to improve design procedures and practices for the future. Although earth embankment dams are constructed with great care and diligence, several serious incidences of dam failure have occurred worldwide (Prasad & Dixit, 2019).

Kayode et al. (2018) explains how many factors have been researched that relate to causing seepage through earth embankment dams. These factors are illustrated in Figure 1.1.

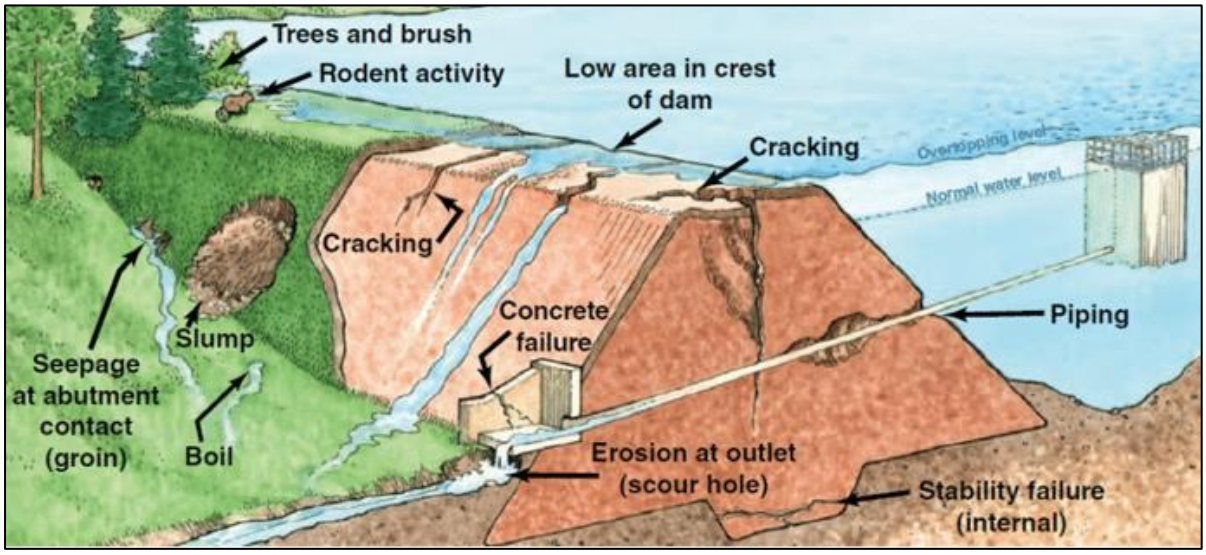

Figure 1.1: *Causes and effects of seepage through earth embankment dams (taken from Kayode et al. (2018)).*

In 1925, two dams were breached and flooded the village of Dolgarrog in North Wales, and sixteen people lost their lives. This disaster led the British parliament to pass the Reservoirs (Safety Provisions) Act 1930. In Wales, this was updated to the Reservoirs Act 1975. This Act covered the safety of all reservoirs in the United Kingdom that could hold at least 10,000 m^3 of water. Under this Act, there are "Panels" (or groups) of civil engineers responsible for checking the safety of reservoirs and dams. Every reservoir must be inspected every ten years by a Panel Engineer, or more often where necessary. Table 1.1 details the features currently investigated at dam sites and what equipment is utilised according to the British Dam Society

(BDS) (British Dam Society, 2022). Panel Engineers are also involved in constructing and remediating new and existing dams and reservoirs.

Table 1.1: *Details of routine dam inspections according to the BDS.*

What is Investigated?	How is it Inspected?
Visual Inspection: • Unusual features such as those illustrated in Figure 1.1 are identified and logged.	• Surface inspection by Panel Engineers performed as part of a site walkover.
Monitor Behaviour: • Seepage and leakage. • Settlement. • Tilting. • Horizontal movements.	• Monitoring dam water level via gauge boards or electronic sensors. • Piezometers within embankment and surrounding area. • V-notch gauges (results continually monitored electronically or periodically by hand). • Elevation of the dams crest as well as lateral movement using GPS and optical instruments. • Pendulums are sometimes installed into vertical shafts within dam structures to monitor tilting.
Floods: • How the reservoir/dam will react to increased water introduced to the catchment (exacerbated by climate change).	• Hydraulic and hydrogeological modelling to ensure the capacity of the dam/reservoir is sufficient. In South Wales, there is also a primary focus on ensuring the capacity of spillways is sufficient.
Earthquakes: • Not so important in the UK. • Tremors can cause major coping stones to shift, and cracks to form in the face of gravity dams constructed from concrete and stone masonry.	• The seismic risk for each site is investigated.

Since reservoir legislation was first introduced, there have been no losses of life due to reservoir failure in Wales. However, the Welsh Government noted that there have been "a number of near-miss incidents where lives could have been lost if a reservoir had failed" (Welsh Government, 2014). Under the Reservoirs Act 1975, the reservoir owner was bound to comply with the legislation irrespective of whether the reservoir posed a threat to the surrounding land. Since then, the Flood and Water Management Act 2010 has amended this statuary framework determining how reservoirs are currently controlled and managed. Owners are now directed to take a more risk-focused approach to reservoir safety. The most notable change to the legislation altered the threshold for what constitutes a "large" raised reservoir from one which is designed to hold 25,000 m^3 of water to one which is designed to hold 10,000 m^3. During the 2010 consultation stage for this legislation, it was noted that there were 203 large, raised reservoirs in Wales. The biennial report to the Minister for Climate Change for the period 01/04/2019 to 31/03/2021, Natural Resources Wales (who are the enforcement authority for the Reservoirs Act 1975 in Wales) reported that there were 371 large, raised reservoirs

registered in Wales. This is an increase of 83%. It was noted in the biennial report that "more work is needed by undertakers to ensure maintenance and safety measures are acted more swiftly and never delayed." Although issues during this period can mainly be attributed to the COVID-19 pandemic, the vast increase in the number of reservoirs which now fall under the Reservoirs Act 1975 cannot be ignored.

Supplementary maintenance and inspection procedures would be incredibly helpful to comply with new legislation. For example, when using traditional inspection techniques, such as visual surveying, the presence of defects such as erosion and burrows can be obscured by dense vegetation, especially during the summer months. As a result, inspections are often conducted in the winter months; however, poorly maintained sites can still have the same problem. The severity of erosion within dam structures can be underestimated due to the seasonal swelling of the soil during these wetter months. In addition to visual surveys, only destructive techniques, such as sampling, trenching, and the drilling of boreholes, can detect erosion at depth (Dyer et al., 2009). Geophysics can provide new characterisation and monitoring approaches which allow the non-invasive detection and characterisation of erosion, seepage, and other water management issues (such as surface drainage) at dam and reservoir sites. Geophysics can characterise dams in terms of their engineered and natural structures, whilst identifying anomalous zones which can be attributed to mechanisms outlined in this section. Geophysics encompasses a non-invasive approach providing negligible risk to suspected vulnerable areas of dams and reservoirs where intrusive investigation may not be appropriate (e.g., drilling boreholes into a suspected weak area of an embankment). Compared to intrusive techniques, geophysics is a relatively inexpensive tool which can provide useful information on its own but can also be utilised to target intrusive investigation and remedial works.

1.2 Case Studies

Since 2006, TerraDat UK Ltd. have funded three geophysical characterisation and monitoring research projects. Key findings and relevant material from these projects are detailed below.

1.2.1 Development of Geoelectric Techniques for Investigation and Monitoring of Landfills (George, 2006)

The aim of this PhD was to put forward ideas for new applications of traditional geophysical techniques to characterise and monitor active and closed landfill sites. The research primarily focused on the application of geoelectrical methods including, but not limited to, Electrical Resistivity Tomography (ERT), ground conductivity and Self-Potential (SP) mapping. George (2006) explains how, much like with dams and reservoirs, there is no legislative requirement for the implementation of geophysical techniques during landfill development, operation, or decommission. The outlook for the research highlights the importance of a multidisciplinary approach to conducting geophysical surveys. George (2006) emphasises the importance of complete spatial data sets to allow for 3D interpretation. George (2006) explains how installing electrode arrays in existing boreholes can allow for easy monitoring solutions by repeating ERT surveys within the field without the need for re-mobilisation of works and equipment.

For closed landfills, George (2006) concludes that by combining ERT, ground conductivity and SP datasets, geoelectrical methods can be correlated and used to plan further intrusive investigations. This mitigates the issue of "non-uniqueness" which can often be a sticking point when interpreting geophysical datasets. In this case, non-uniqueness is used to describe how certain anomalous features (i.e., conductive zones in an ERT profile), can be attributed to multiple potential sources. George (2006) produced a conceptual site model combining all these datasets into one cohesive interpretation. The presence of landfill capping structures was

identified as a significant constraint on the effectiveness of geoelectrical methods in this scenario, highlighting the importance of obtaining all pre-existing information pertaining to a site prior to data collection and interpretation.

For an active landfill setting, George (2006) concludes that ERT is a significant geophysical tool for characterising landfill waste. It is explained how the method needed to be adapted due to constraints relating to poor resolution and accuracy with increasing depth in active landfill settings. ERT electrodes were installed into a cell drainage medium prior to waste emplacement and were used in conjunction with ground surface electrodes above the waste-mass. This method enabled the delineation of basal leachate accumulation and differentiate perched water tables within the landfill waste. ERT characterisation in this manor was attempted in a single 2D plane. George (2006) explains how further development of such techniques should include the installation of multiple basal arrays in conjunction with traditional surface non-intrusive methodologies to enable 3D analysis of resistivity data, thus characterising the whole waste mass.

For monitoring landfill restoration, George (2006) proposed a system of permanently installing vertical electrode arrays during routine placement of gas extraction boreholes prior to site restoration. It was concluded that the traditional approach of gas well leachate dipping was not providing an accurate representation of the depth of perched tables within the landfill study site.

1.2.2 The Development of Integrated High-Resolution Geophysical, Photogrammetric and GPS Surveying Applied to Landslides in the South Wales Coalfield (Taboga, 2011)

As with the previous project, a multidisciplinary geophysical approach was utilised to solve a geotechnical/geo-environmental problem. In this case, the aim was to characterise and monitor the Mydydd yr Eglwys landslide in South Wales. In this instance, a broader array of geophysical techniques was used, notable additions being that of Seismic Refraction and Multichannel Analysis of Surface Waves (MASW). Other techniques such as digital photogrammetry and GPS positional surveying were also utilised.

A ground conductivity survey delineated clay/moisture rich/deficient zones. The inclusion of Induced Polarisation (IP) surveys was considered necessary to delineate clay rich/deficient zones from moisture rich/deficient zones. An SP survey provided information pertaining to groundwater flow beneath the slope. Flow was identified towards the main scarp of the landslide, at the toe, and within a major fault cutting through the site. Several short wavelength anomalies were also associated with the most active area of the landslide. Seismic results were less informative. The technique was able to describe the gradual decrease in the degree of fracturing with depth. The results imply that the surface of the rupture toe was 4 mBGL – 5 mBGL, however, borehole data suggested that the surface rupture was a lot shallower. MASW identified a 1 m – 5 m thick layer of low shear velocity material which corresponded to highly weathered and/or clay rich material in borehole data. Taboga (2011) concludes that ERT was the most effective technique deployed at the site. Interpretation allowed for the delineation of lithologies and areas of increase clay and/or moisture content (IP was necessary to delineate between these conductive features). Correlation with SP datasets allowed the direction and extent of subsurface water flow to be identified. This information was compiled into a site conceptual model of the landslide.

The landslide was monitored by repeating ERT surveys multiple times. By observing changes in resistivity, Taboga (2006) explains how repeated ERT surveys are useful for detecting temporal changes in groundwater content and detecting preferential seepage pathways. Taboga (2006) further explains how this technique could be improved by increasing the frequency of ERT surveys via a permanent installation. This in combination with reliable local rainfall data and the monitoring of borehole water levels would provide a more effective solution.

1.2.3 Next Generation Monitoring of Critical Welsh Infrastructure: Creating a Starting Point for Integrating Remote Monitoring Data (Farnham, 2021)

This project is perhaps the most closely linked to this research project. Results from Farnham (2021) provided the baseline infrastructure necessary for handling long-term remote data collection. Farnham (2021) explains how despite the frequent use of geophysical techniques and remote sensing for solving geotechnical and geo-environmental problems, there is no one existing system that applies these to monitoring critical infrastructure in Wales. The aim of the project was to combine a range of near-surface geophysical techniques, with other spatial sensing platforms such as InSAR to monitor Welsh reservoirs for leaks and other structural problems.

Farnham (2021) successfully created a functioning early version of a monitoring system and applied it to two sites in Wales. The system utilised automated SP measurements and uploaded these measurements to a dashboard. Data was able to be collected regularly from the Barlwyd site and Fourier analysis was conducted to remove temporal variations (noise) due to temperature. This filtered data was made accessible through the developed dashboard and allowed for integration with InSAR datasets.

More recently, a second system was removed from a Dŵr Cymru Welsh Water site (site to remain anomalous) after the completion of this project. Data from this system showed a clear connection between reservoir level and SP response indicating a preferential seepage pathway towards the top of the crest. It was hypothesised that this pathway was attributed to a more granular layer of material within the upper section of the embankment. Recent intrusive investigation has since confirmed the presence of a gravel layer within the upper section of the embankment which is acting as a preferential seepage pathway. The elevation of this gravel layer also corresponded with the elevation of the reservoir water when an SP response was observed. The early identification of this problem area enabled the owner of the dam to conduct more targeted intrusive investigation works, saving them time, money, and effort.

1.3 Geophysical Techniques for Characterising Earth Embankment Dams

The aim of geophysically characterising earth embankment dams is to obtain a snapshot of the distribution and composition of materials that make up the dam/embankment, the condition of these materials and relate them to the surrounding area. Specifically, the aim is to characterise things such as:

- The distribution of materials across the dam, both shallow and at depth.
- Depth to natural strata (bedrock).
- Areas of increased moisture content.
- Location of surface drainage features, either intentional or not (i.e., French drains).
- Location of any existing infrastructure (pipes, concrete pads, piezometers etc).
- Voiding under spillways.

A multidisciplinary approach to the geophysical characterisation of earth embankment dams is the most effective. Unlike other more traditional site investigation techniques, such as the drilling of boreholes and conducting Standard Penetration Tests (SPT's) (more information see Knappett and Craig (2012)), there is an issue of "non-uniqueness" associated with geophysical surveys. In this case, non-uniqueness refers to the fact that with most geophysical techniques, contrasts, anomalies, and trends in datasets can be attributed to multiple sources. For example, a common pitfall of ground conductivity and ERT surveys is that it cannot be confirmed whether a conductive zone is attributed to a variation in the natural subsurface conditions (increased moisture content etc) or buried ferrous material without intrusive investigation. Other than intrusive investigation the best way to combat this non-uniqueness is to combine multiple geophysical techniques. A common example of this is combining ground conductivity and magnetometry datasets to rule out sources of buried ferrous material. By doing so, conductive areas can be attributed to variations in subsurface conditions such as increased clay and/or moisture content.

A sticking point in the interpretation of electromagnetic methods is often the delineation between areas of increased clay and increased moisture content. The inclusion of an Induced Polarisation (IP) survey within this project aims to evaluate this distinction, creating a more definitive conceptual site model of the site.

For further information pertaining to the details of each geophysical technique outlined below (and in Chapter 6), the reader is advised to refer initially to Milson and Eriksen (2011), and for more in-depth information to Reynolds (2011).

1.3.1 Ground Conductivity

Ground conductivity surveys involve introducing an electromagnetic field into the subsurface and recording the corresponding returning signal with the same apparatus. Ground conductivity data is acquired across a grid and produces a grid of spatial data which is presented as a plan of conductivity in mS/m. It should be noted that for each given survey point, the value recorded is a bulk value of the conductivity of the ~ 3 mBGL – 5 mBGL of material directly below the survey point. As a result, it is not possible to infer conductive sources at depths greater than this.

Data can be acquired by one field operative. For this project, a Geophex GEM-2 system was used. The equipment includes a "ski-like" plank which is slung over the operatives shoulder, which is in turn linked to a GPS (see Figure 1.2). The apparatus is then walked along parallel survey lines at a spacing of 2 m across the area of interest. Data is recorded at user defined intervals (often every second). Data is recorded by a logger, compiled, and filtered to remove rogue values using WINGEM-3 (proprietary software for the GEM-2 instrument). Data is then exported as a XYZ file and processed in Oasis Montaj.

Due to the nature of data acquisition, it is possible to cover large areas in a relatively short period of time. Although not possible to acquired data at great depth, the presentation of spatial data makes ground conductivity useful for identifying the composition of engineered material often making up the top layer of earth embankment dams, as well as any areas of intentional or non-intentional surface drainage. The reciprocal of conductivity data can also be calculated to present the data as resistivity (Ωm) to allow for comparative interpretation with ERT datasets.

Figure 1.2: *Photograph of ground conductivity (left) and magnetic data acquisition (right).*

Conductive zones infer clay-rich material and/or moisture-rich and/or ferrous material. Resistive zones (areas of low conductivity), infer clay deficient, and/or dry and/or granular material. The potential for ferrous material can eliminate by performing a magnetometry survey.

Sentenac et al. (2018) conducted a ground conductivity survey of an embankment dam using the same equipment (GEM-2). The method allowed the researchers to develop a basic description of material homogeneity and problematic zones. Interpretation of this data was then used to identify areas to be further investigated by ERT and SP techniques. Although not partnered with a magnetic survey, comparison between ERT and SP datasets showed that the ground conductivity survey did not miss any electromagnetic anomalies at the site.

1.3.2 Magnetometry

Magnetic surveys aim to identify buried ferrous material. This can range from identifying buried services such as pipes and cables, to highly accurate archaeological mapping. The main aim of conducting a magnetic survey for this project is to identify any ferrous structures, objects, or debris within the downstream shoulder of the embankment which may affect the results and interpretation of ground conductivity, ERT, IP surveys and SP monitoring. Iron and steel are ferromagnetic and are usually strongly magnetised. Even small steel objects can produce fields with magnitudes of hundreds of nanoteslas. However, the fields produced by small objects decrease rapidly with depth below the ground surface.

Data is acquired in a very similar way to ground conductivity data (Figure 1.2). For this project, a SENSYS MagWalk magnetometer was used to acquire gradiometric data continuously along a series of 2 m spaced parallel survey lines over the embankment. Like the GEM-2 instrument, the MagWalk apparatus is connected to a GPS, and the data is recorded by a logger. Data was downloaded and compiled from the instrument using the MagDrone Data Tool provided by SENSYS. Initial data processing and filtering was performed using this software. The rest of the data was processed in the same way as the ground conductivity data.

The effect of shallow sub surface ferrous material and can be eliminated by comparing magnetometry and ground conductivity data for the same area. It is also possible to identify any unmapped dam infrastructure such as pipework

1.3.3 Electrical Resistivity Tomography (ERT)

Electrical Resistivity Tomography (ERT) has been used to successfully detect preferential seepage pathways through earth embankment dams (Panthulu et al., 2001). ERT involves the injection of a direct current into the subsurface and the subsequent measurement of potential differences using various electrode spacings and configurations. ERT datasets are commonly presented as 2D pseudo-sections (slices) of the subsurface. This provides information pertaining to the distribution of resistive material at depth. The maximum depth of the survey is limited by the maximum electrode spacing used to acquire the data. Due to the nature in which the data is acquired, a "clipping" of ERT pseudo-sections is observed at their edges. This means that at the maximum depth, only one data point is recorded, and the edges of the pseudo sections are not vertical (the angle of clipping depends on the minimum electrode spacing). Care must also be taken in interpreting data at depth as the density of data points reduces.

Much like ground conductivity data, less resistive zones infer clay-rich material and/or increased moisture and/or ferrous material. More resistive zones infer clay deficient, and/or dry and/or granular material. Table 1.2 shows a simplified relationship between resistivity, conductivity, and typical geological setting. Figure 1.3 illustrates typical resistivity (and conductivity) value ranges for different common geological units. As explained in Revil et al. (2014), two contributions control the electrical resistivity of porous soils. The first is the conduction through the bulk pore space, and the second is the conduction through the electrical double layer coating the surface of soil grains. Therefore, although limited in how well these data sets can be interpreted, they provide a useful insight into the composition and variation in homogenous material comprising most earth embankment dams.

Table 1.2: *Simplified relationship between resistivity, conductivity, and subsurface material.*

Resistivity (Ωm)	Conductivity (mS/m)	Typical Geological Setting
High	Low	Dry, granular clay-deficient material. Air-filled voids, competent bedrock
Intermediate	Intermediate	Mixed/damp sediments, weathered bedrock
Low	High	Clay-rich lithologies, water-saturated sediments

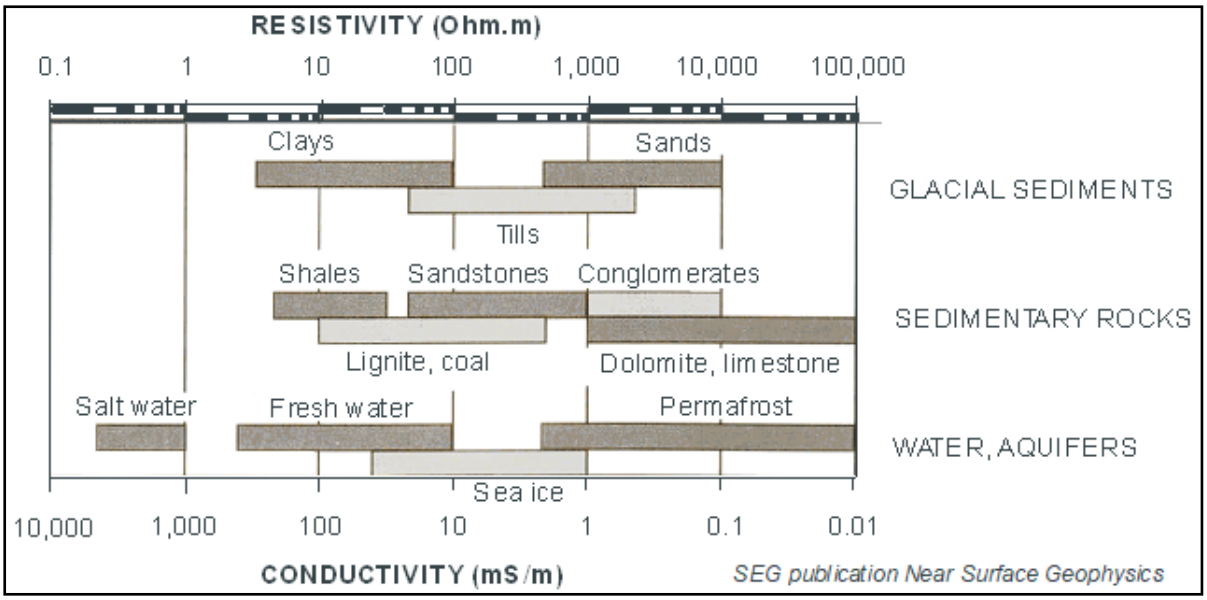

Figure 1.3: *Ranges of resistivity and conductivity values of typical sedimentary materials* (SEG, 2022).

Groups of four electrodes are used for taking resistivity measurements. These groups are known as quadrupoles. Figure 1.4 illustrates a typical electrode configuration for an ERT survey. Current is injected into the subsurface through electrodes A and B, and a potential difference is measured between electrodes M and N. For this project, an IRIS Syscal resistivity system (Figure 1.5) was used. This system allows for four 18 channel cables to be connected to 72 steel electrodes. Utilising a minimum electrode spacing of 2 m, a maximum depth of ~ 20 mBGL is achievable across the centre of each profile. It is also possible to extend the chainage of each survey line by "rolling-on" the first cable in each survey, allowing for a pseudo section with a consistent maximum depth of ~ 20 mBGL. To ensure good contact resistance between adjacent pairs of electrodes, a resistance check function integrated into the IRIS instrument was used. Contact resistances were kept bellow 2 kΩ by "watering-in" electrodes and surrounding them with bentonite clay where necessary.

The resistivity obtained through this method is referred to as apparent resistivity. This is due to the medium in which the current is passing through not being perfectly homogeneous. To obtain true resistivity data from apparent resistivity, datasets must go through a process known as inversion. In summary, apparent resistivity data is processed using a finite difference network. This network compares an initial resistivity model based on the recorded apparent resistivity, to a theoretical pseudo-section. Differences between the theoretical model and the observed apparent resistivity are then used to make changes to the true resistivity of each data point accordingly. This process is repeated until the RMS error between the models reaches an appropriate value (e.g., 10%). Both Res2Dinv and ResIPy was used to invert ERT datasets, allowing for topographic variation. This data was then exported to Surfer, where it was gridded, contoured, and presented as 2D pseudo-sections.

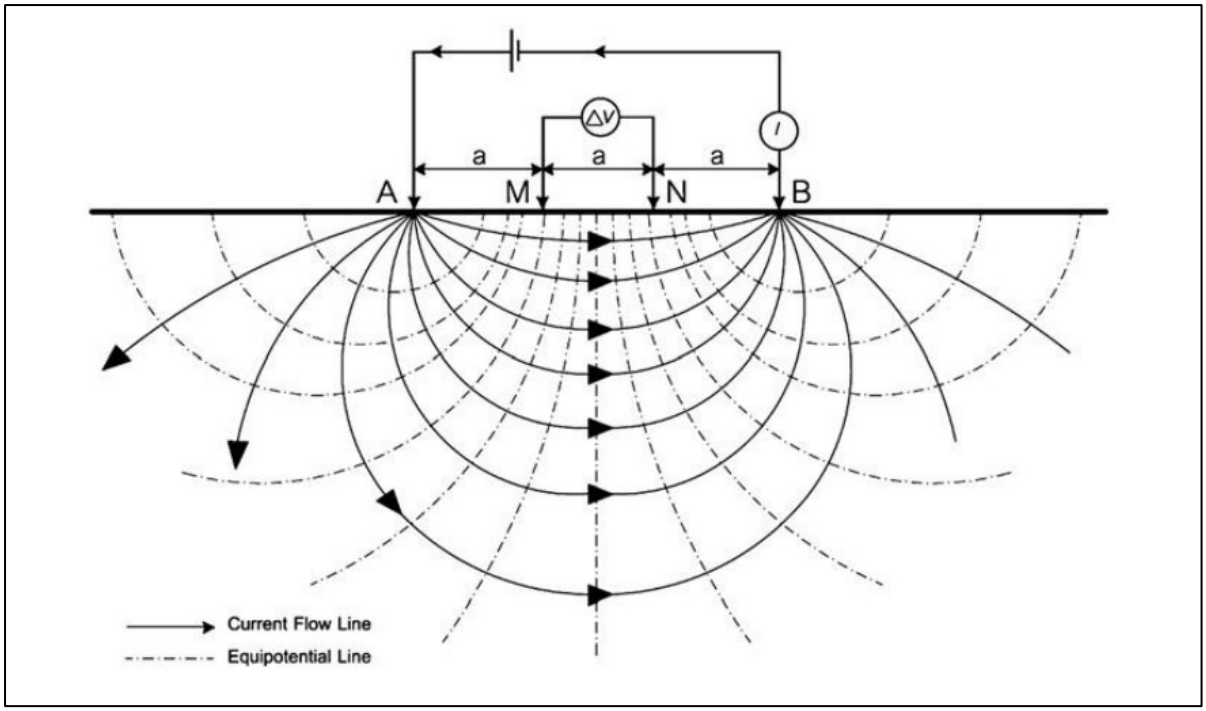

Figure 1.4: *Electrode configuration for Electrical Resistivity Tomography showing lines of equipotential (Reynolds, 2011).*

Figure 1.5: *Acquisition of ERT and IP data using an Iris SYSCAL resistivity system (library photo from TerraDat UK Ltd.).*

ERT data was acquired using a Wenner-Schlumberger arrangement (arrangement shown in Figure 1.4). Dahlin and Zhou (2004) show that this configuration provides good signal to noise ratio and good signal strength at depth. This configuration also has a high vertical resolution making it ideal for identifying horizontal features such as boundaries between horizontal strata and sub-horizontal potential seepage pathways. An alternative configuration commonly used is a dipole-dipole arrangement. This configuration places the potential electrodes outside of the current electrodes and is better at locating vertical and dipping structures.

Multiple ERT profiles are often taken parallel to the crest of embankment dams to link features and identify the alignment of potential preferential seepage pathways. These datasets are increasingly being presented in 3D, using GIS packages. It is also possible to invert 2D ERT sections together to produce a 3D model. It is now possible to achieve this using open-source software such as ResIPy and ParaView. Visualising ERT profiles in this way provides valuable insight into existing datasets at limited extra cost when compared to standard processing and presentation methods.

1.3.3.1 Quantifying Error in ERT Datasets

Measurement errors play an integral part in processing ERT data, affecting the amount of dampening imposed on the data and the point at which convergence is attained. Weighting data in the objective function achieve both; therefore, measurement error estimates allow for the over or underfitting of data during the inversion process. It is possible to account for errors using robust inversion and Bayesian inversion methods, which account for outlying data and data uncertainty functions. However, an accurate prescription of measurement errors is still essential to obtaining reliable and realistic inversion results (Tso et al., 2017).

The two most common methods of obtaining measurement errors are repeatability and reciprocity. Repeatability errors are acquired through stacking (often called stacking errors), i.e., the repeated measurement of transfer resistance through numerous cycles of current injection. Stacking errors are commonly used in ERT surveys as most modern instruments are equipped with stacking capability. This is attractive for commercial use as surveys are often time-sensitive and time-consuming. Stacking errors are helpful in quality assurance and quality control and form another basis for editing datasets before inversion (e.g., eliminating bad data points). However, repeatability errors provide minimal insight into data weightings for ERT inversion.

Reciprocity errors rely on the scientific principle that changing source and observation locations should yield the same response. For the case of ERT, current and potential electrode positions are swapped for the same quadripole measurement (e.g., A and B are swapped for M and N). Reciprocal error, R_{error}, is calculated from the difference between the direct and reciprocal measurement of the same data point using the following equation:

$$R_{Error} = abs\left(\frac{N - R}{N}\right)$$

Equation 1.1

Where N and R are the direct and reciprocal measurements respectably (Mwakanyamale et al., 2012). Reciprocity breaks down when the ground does not respond linearly (i.e., non-ohmic) or when measurements are time-dependent (reciprocal measurements should be taken immediately after direct measurements). Reciprocal measurements provide a better quantification of noise than stacking errors (Binley et al., 1995).

It should be noted that although useful, repeated, and reciprocal measurements are not measurements of accuracy but precision. Sources of systematic error are not accounted for explicitly by either, with some methods attributing them to random errors whilst others miss them altogether. An advantage of reciprocal errors is that some of this systematic error is accounted for in swapping the electrode positions. However, changing the number of cables in an array over multiple surveys makes this symptom less useful (LaBrecque et al., 1996).

Tso et al. (2017) found that reciprocity was the most common error analysis method used in studies involving the use of ERT. Studies often attributed the exclusion of reciprocal errors to logistical constraints and argued that stacking errors are efficient. A common approach is to create an error model of reciprocal data and apply this model to other datasets. This was the approach adopted to process ERT data for this project.

All ERT datasets were subject to the following quality assurance and quality control procedures:

1. First stage filtering in Prosys II. Resistance values > 0 Ω, as well as data points with a standard deviation of resistance < 3 Ω, were neglected.
2. All values of resistance were attributed with a reciprocal error approximation (data weighting) from reciprocal analysis of ERT 9 in ResIPy (explained below).
3. In RES2DINV, there is an option to exterminate bad data points.

ERT 9 was repeated to obtain reciprocal measurements. The analysis of these reciprocal measurements was performed in ResIPy, which follows the approach described in Mwakanyamale et al. (2012). Reciprocal errors are binned into 20 bins of equal count and sorted based on the average resistance error, $R_{Average}$, given by:

$$R_{Average} = \frac{|R_{Direct} + R_{Reciprocal}|}{2}$$

Equation 1.2

Where R_{Direct} and $R_{Reciprocal}$ correspond to the resistance measured directly and through reciprocal measurements, respectively. For each bin, the average of the reciprocal errors was calculated and used to represent that sample of data. An empirical approach follows this process, applying the simplest function that adequately captures the variation in error over the measurement range. ResIPy uses either linear or power-law fits. ERT 9 was selected to create the error model as it intersects the downstream embankment's conductive "homogeneous" regions and the resistive anomaly identified by previous surveys (see Section 5).

The power-law resistance model resulting from the procedure explained above in ResIPy can be seen in Figure 1.6 (note logarithmic axis). A power-law function can represent this model ($R^2 = 0.931$):

$$R_{Error} = 0.003 R_{Averagge}^{0.929}$$

Equation 1.3

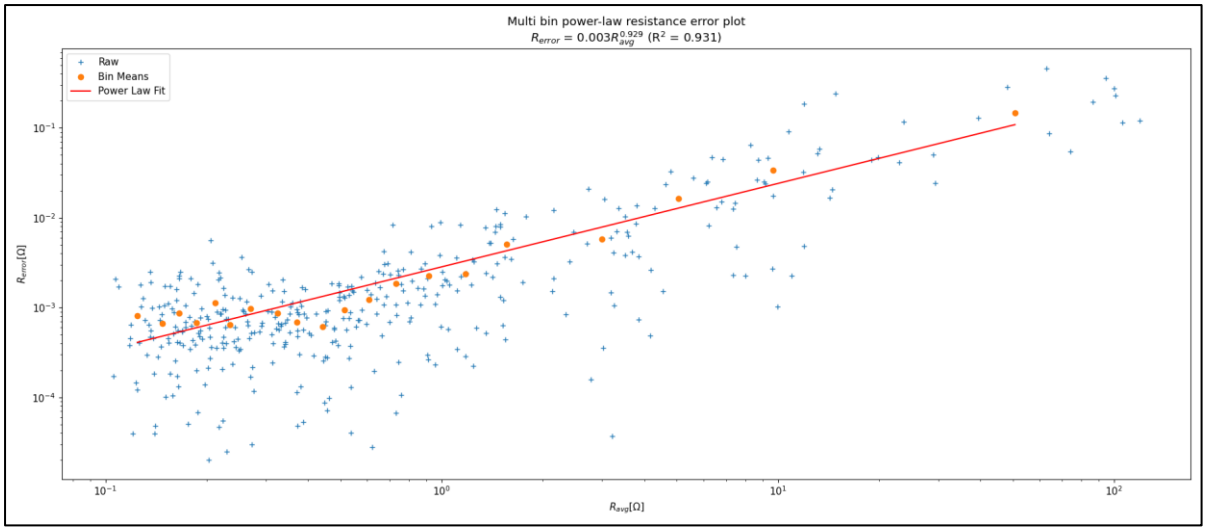

Figure 1.6: *Results of multi-bin power-law resistance error model. Power law fit equation used to model error values for all ERT datasets.*

This model was used to estimate the error for all other ERT datasets. Values of resistance were made the subject of the power-law function, producing a corresponding error value. This approach strikes a balance between statistical valid error modelling and practical application.

1.3.4 Induced Polarisation (IP)

Induced Polarisation (IP) is effectively a measurement of the capacitance of the subsurface (i.e., how well the ground "holds-on" to charge). IP is primarily utilised for detecting disseminated metal ores, especially, bedded lead/zinc and sulphide-related gold deposits. IP is also used to detect groundwater and is used in geothermal exploration. The use of IP methods in environmental applications has increased in popularity since the 1990s (Reynolds, 2011).

An IP survey involves the injection of direct electrical current at various electrode spacings along a profile and the subsequent measurement of the time taken for the induced charge to dissipate. This allows the computation of the chargeability of the ground (capacitance). The IP data is recorded with the same IRIS Syscal system at the same time as the ERT survey. The field deployment of the electrodes and the electrode geometry (72 electrodes spaced 2 m apart) are identical to that described in Section 1.3.3. A chargeability cross-section of the subsurface is then derived from the recorded data. IP is useful in dam investigations as it can distinguish between the non-unique ERT responses that derive from moisture rich or clay rich material.

From chargeability datasets, it is possible to compute the normalised chargeability. Slater and Lesmes (2002) explains how typical IP interpretation in terms of conventional IP parameters, such as chargeability, is limited by the fact these parameters are affected by both conduction through the bulk pore space, and the conduction through the electrical double layer coating the surface of soil grains (Revil et al., 2014). Normalised chargeability quantifies the magnitude of surface polarisation processes. This is achieved by dividing the chargeability by the magnitude of resistivity (Equation 1.4). As IP surveys can take place alongside conventional ERT surveys, data acquisition and computation take minimal effort and time.

$$M_n = \frac{M}{\rho}$$

Equation 1.4

Another advantage of normalised chargeability is that it is proportional to quadrature conductivity, allowing for direct comparison with ERT cross-sections (conductivity profiles can be computed easily from ERT cross-sections by taking the inverse of every data point). For non-metallic materials, quadrature conductivity and normalised chargeability are closely related to lithology. Slater and Lesmes (2002) looked at the dependence of normalised chargeability on salinity and clay content. They were able to segment resistivity cross sections into relatively clay rich and clay deficient zones.

By delineating between clay rich and clay deficient zones, the issue of non-uniqueness between clay rich/deficient and moisture rich/deficient zones is mitigated.. If a zone is displaying relatively low resistivity values, but relatively high normalised chargeability values, it can be assumed that increased conductivity is being caused by increased clay content within the subsurface. For a zone with relatively low resistivity values, and relatively low normalised chargeability values, this increase in conductivity is more likely to be caused by increased moisture content.

For this project, the data was processed using Res2Dinv software to derive modelled chargeability cross-sections of the subsurface. This data was then exported to Surfer 9 where it was gridded and presented as a 2D cross-section of chargeability. The normalised chargeability was computed in Surfer 9 using the grid-math tool.

A plot of normalised chargeability against quadrature conductivity was used to set binary values to indicate the spatial distribution of clay rich and clay deficient material (Figure 1.7). Normalised chargeability values greater than 0.25 mS/m are considered clay-rich, and values less than 0.25 mS/m are considered clay-deficient. These thresholds were taken from Slater and Lesmes (2002).

For this project, time-domain measurements of IP were taken. This method involves the injection of current into the subsurface and the computation of a decay curve for a given period after the current is switched off. When the applied current is switched off, the voltage drops instantaneously, resulting in the remaining voltage to decay with time. Alternative methods of measuring IP include frequency domain IP measurements (more information can be found in Reynolds (2019)).

Abdulsamad et al. (2019) used ERT, IP and SP techniques to provide reliable information pertaining to the detection of leakages in dams and embankments. It was concluded that ERT alone was unable to distinguish between the two main contributors to the electrical conductivity of rocks and soils; the bulk conductivity associated with current flow through the pore network and the medium; and the surface conductivity associated with the conduction in the electrical double layer coating the surface of grains. It is explained that by combining ERT and IP (normalised chargeability) the separation of these two contributions was possible, thus gaining an insight into the water content (or lack thereof) without making assumptions regarding the amplitude of surface conductivity of the soil or rock grains. It was concluded that combining IP with ground conductivity and SP surveys was the most workable solution. SP can be used first to identify potential leakage pathways, and then IP and ground conductivity surveys can be used to estimate water content and saturation values.

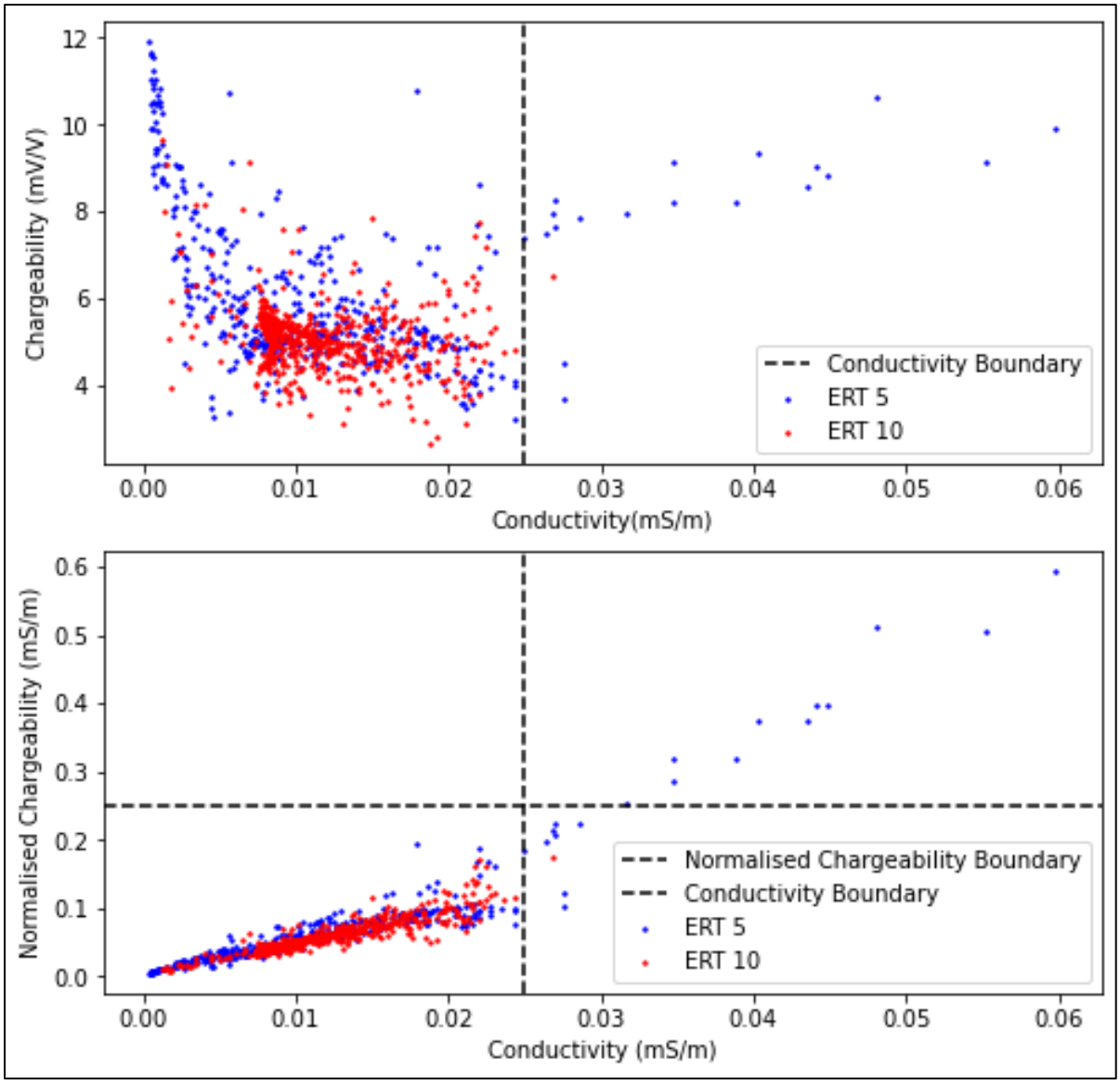

Figure 1.7: Top: Plot of chargeability against conductivity for ERT 5 and ERT 10. **Bottom:** Plot of normalised chargeability against conductivity for ERT 5 and ERT 10. Values on either side of the conductivity boundary are distinguished by calculating the normalised chargeability. The normalised chargeability boundary was determined following Slater and Lesmes (2002).

1.3.5 Self-Potential (SP)

The electrical Self-Potential (SP) method is an example of a passive geophysical technique. The SP method has been used extensively in mineral exploration (Schlumberger & Schlumberger, 1922), groundwater and geothermal investigations, and many other applications (see Reynolds (2019)). In recent years, the SP method has been applied to various environmental studies such as bioremediation and monitoring fluid contamination (Kulessa et al., 2006) and (Cui et al., 2017). The SP method is unique in the sense that it is the only geophysical method that can directly detect subsurface water flow. This attribute makes it an ideal technique for detecting seepage through earth embankment dams.

The SP method is considered one of the cheapest near-surface geophysical techniques in terms of equipment and is among the simplest to apply in the field. SP measurements are taken using

non-polarising electrodes connected to a voltmeter. A metal forms a non-polarising electrode when it is in contact with its own salt (e.g., copper and copper sulphate, or lead and lead chloride). The metal is suspended in a saturated salt solution which is allowed to percolate through the electrode's (pot's) porous base, creating an electrical coupling with the ground. The potential difference between two non-polarising electrodes is measured using a voltmeter with high sensitivity (~ 0.1 mV) and a high input impedance ~ 10 MΩ – 100 MΩ. By convention, a reference electrode is connected to the negative terminal of the voltmeter (Revil & Jardani, 2013).

There are two main field techniques for mapping SP fields. The potential gradient method consists of using two electrodes at a fixed distance. Measurements are attributed to the midpoint of the two electrodes, and the potential gradient is calculated by dividing the potential difference measured by the electrode separation (units Vm^{-1}). These two electrodes are then "leap-frogged" along a traverse, ensuring that the potential's polarity is being recorded as well as the amplitude. Alternatively, the potential amplitude method keeps one electrode at a fixed location (base), and then the potential difference (units V) is recorded with respect to a roaming measurement electrode. The base electrode is kept in a small hole filled with bentonite. Due to the presence of bentonite modifying the electrical potential at the contact between the electrode and the ground, the potential at this station is considered to be arbitrary. Unlike other techniques, such as ERT, improving the coupling between the electrode and the ground using salt water should be avoided (especially for monitoring purposes). Evaporation changes the salinity of the porewater, generating spurious changes in electrical potential over time. These changes are attributed to diffusion potentials. The roaming measurement electrode measures the electric potential at a set of stations, spatially referenced using a GPS. It is recommended that prior to, and after, each measurement the difference between the reference electrode and the roaming electrode is recorded by making contact between the electrodes through their porous membranes. This voltage is known as the drift voltage and is used to correct raw SP data for the drift of the reference electrode. Drift voltages can arise for several reasons including the salt soaking into the ground altering the electrodes coupling, and the effects of temperature variation. The temperature coefficient of copper-copper sulphate is approximately 0.5 mV/°C. This can generate a difference in potential greater than 10 mV. For SP mapping, these temperature gradients often arise from the roaming electrode held in someone's hand and the reference electrode situated in the cooler ground. Measures can be taken to avoid such temperature differences between electrodes. For example, the roaming electrode can be attached to a stick to avoid direct contact with hands (Revil & Jardani, 2013). Barde-Cabusson et al. (2020) developed a practical approach for SP data acquisition that considers such factors and prioritises control measures to make data acquisition practical.

Voltages recorded at the surface are summations of voltages generated by subsurface water flow, known as streaming potentials (SP_{Stream}), and other processes such as temperature changes, atmospheric effects, and the geology/geochemistry of the subsurface. As the only concern is with the effects of streaming potentials, these additional processes can be summarised by a noise term (SP_{Noise}).

$$SP_{Measured} = SP_{Stream} + \int SP_{Noise}$$

Equation 1.5

When water, acting as an electrolyte or a solvent, flows through a porous matrix, an SP signal is generated. An electrokinetic potential (E_K) forms due to an electrolyte flowing through a capillary or porous medium. This creates a dipolar charge separation (Ahmad, 1961). A

gradient of electrical potential forms as porewater usually contains an excess of charge (Q_v). This excess charge forms due to the interaction between the moving porewater and the electrical triple layer. Figure 1.8 illustrates the electrical triple layer at the soil-water interface.

The amplitudes of streaming potentials decay as a function of depth. As a result, topographic highs and lows are generally associated with positive and negative SP anomalies, respectively (Revil et al., 2003). Electrical charge flows in the opposite direction to fluid flow, with the SP signal becoming more positive in the direction of water flow. This phenomenon will be exaggerated after periods of surface recharge in the form of rain or snowmelt. In significantly uneven surface relief areas, the measured SP signal can be distorted in current flow patterns. Near-surface resistivity can vary significantly from point to point, affecting the flow of charge through the subsurface and introducing further noise in SP measurements (Corwin & Hoover, 1979).

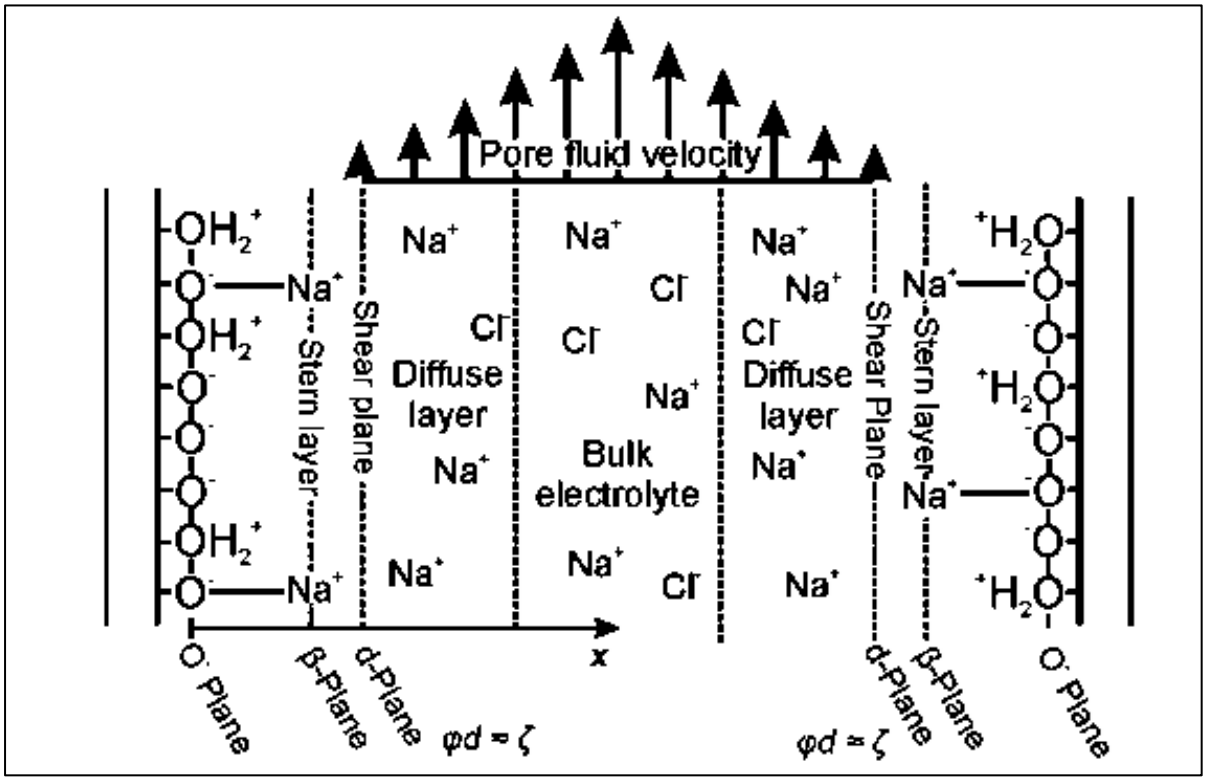

Figure 1.8: *The electrical triple layer at the soil-water interface (Revil et al., 2003).*

SP mapping has been used extensively to detect preferential flow pathways through earth embankment dams. The first notable example of this is observed in Ogilvy et al. (1969). Other notable examples include Gex (1980), Sheffer and Howie (2001, 2003), and Panthulu et al. (2001). Typically, steady-state SP anomalies associated with earth embankment dams amount to several tens of millivolts (32 mV for the dam investigated in Panthulu et al. (2001) and 80 mV for the dam investigated in Bolève et al. (2009). However, in some situations, steady-state anomalies can exceed several hundred millivolts, as was the case in Rozycki et al. (2006), where an anomaly of 300 mV was measured.

Wilt and Corwin (1988) explains that variations of the measured SP above and along a seepage pathway is a complicated function of the geoelectrical section; electrokinetic coupling coefficients; flow rates; and the depth and geometry of the flow path. However, Butler and

Llopis (1990) provides a quantitative description of measured SP variation along a seepage pathway. Observations and modelling indicated that:

1. Negative SP anomalies can be associated with areas where seepage is entering or penetrating through the dam. Negative SP anomalies can also be found above seepage pathways where the flow is horizontal or descending.

2. Positive SP anomalies can be associated with areas where flow is ascending, and surface seepage occurs.

In plan view, a complete SP anomaly associated with a localized seepage pathway through or under a dam will often consist of a closed negative anomaly around the seepage entrance; a closed positive anomaly around the seepage exit; and a zero-anomaly contour or zone between the two closures. Therefore, depending on SP measurement locations (relative to the seepage pathway), the measured SP field may be a negative or positive trend. Figure 1.9 illustrates the concept of detecting seepage through or under dams using a single survey line and its expected resulting SP profile. This type of SP profile is observed in Bolève et al. (2009).

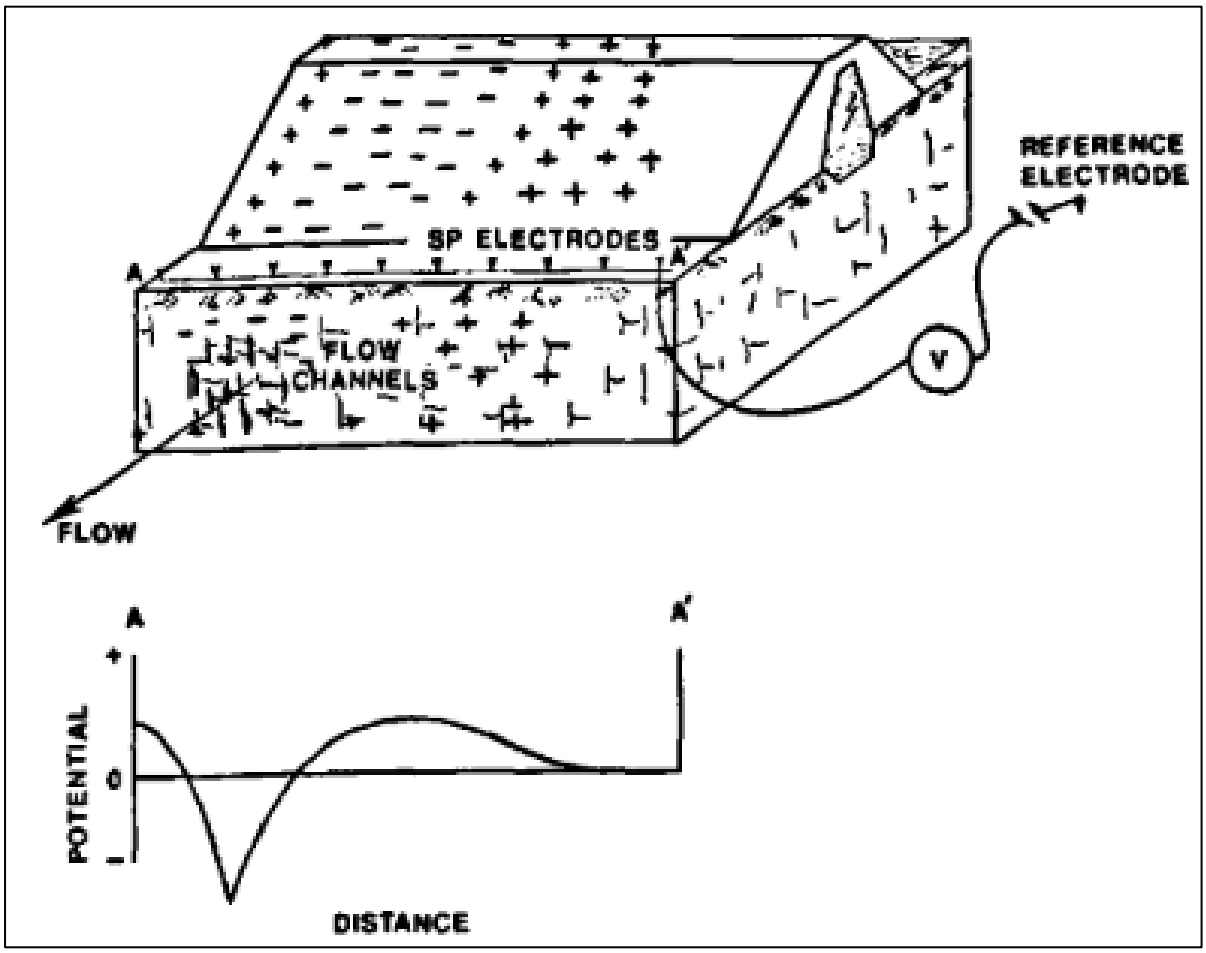

Figure 1.9: *Illustration of the concepts of self-potential (SP) anomaly generation and of fixed-reference SP surveys* (Butler & Llopis, 1990).

1.4 Self-Potential Monitoring (SP Monitoring)

The SP method can be used to monitor changes in variables such as Darcy velocity, moisture content and salinity. For monitoring applications, a multi-electrode array is connected to a multi-channel or multiplexed voltmeter. Electrode arrays are then installed around areas of interest, either as profiles to intersect anomalies or as grids to allow contour maps to be produced (Revil & Jardani, 2013).

As outlined previously, all non-polarising electrodes have a temperature dependence. For monitoring, the shallow subsurface is always characterised by a diurnal temperature variation to a depth of approximately 30 cm - 50 cm. Therefore, electrodes should always be buried to at least this depth. Otherwise, a temperature sensor would be required to be installed within the vicinity of each electrode to allow for a post-measurement correction. Burying electrodes has several other advantages. It limits the influence of external electromagnetic noise (the sensitivity of which decreases rapidly with depth); reduces the risk of desiccation; and avoids spurious electrical signals associated with the roots of vegetation (Revil & Jardani, 2013).

For monitoring, it is necessary to take measurements at the same locations over weeks, months, and years. It is not recommended to leave electrodes in place for extended periods because they tend to drift over time. However, repeat return visits are not practical for most situations where monitoring is required (especially in a commercial environment). A way to overcome this challenge is to pack SP measurement stations with a bentonite plug. Installing electrodes into a bentonite plug, and sealing the top with a plastic cap, protects the electrode from draining too quickly into the soil. This approach has been proven to be extremely precise (accurate to ± 1 mV or better) for repeat readings over time (Revil & Jardani, 2013).

Little research has been conducted monitoring passive SP fields produced by seepage through embankments. The method which as seen the most extensive research involves injecting salt tracers upstream of observed seepages. SP measurements are then monitored to identify responses and detect potential preferential seepage pathways. These tests are known as “SMART” (Self-Potential Monitored Salt Tracer Tests) (Revil & Jardani, 2013).

The obvious advantage of SP monitoring is that it allows the field to be mapped over time. When combined with external datasets such as reservoir level, meteorological events, piezometer levels and flow rates, it is clear to see how it can be a powerful tool. In addition, it is possible to combine SP and ERT datasets to image preferential seepage pathways using SP tomography. SP tomography is explained in Bolève et al. (2009). The method involves inverting SP data with ERT and topography datasets to detect preferential seepage pathways. SP and ERT datasets can be inverted together to obtain current source density. It is possible to calculate seepage velocities (Darcy velocities) associated with calculated current distributions. Additional information such as fluid conductivity, permeability, and water heads can function as boundary conditions to increase the models accuracy. It is possible to apply algorithms, such as those developed in Bolève et al. (2009) to achieve this. However, the process is complicated and requires expensive finite element code, such as Comsol Multiphysics used in Bolève et al. (2009). However, some software packages now allow for the importation of SP and ERT datasets in commercially recognised formats (e.g., Microsoft Excel workbooks of SP data and .INV files from Res2Dinv) to be included in inversion. An example of this is Zond’s SP2D software. The program allows the user to solve direct and inverse problems using the natural field method. This uses the finite element method, where the behaviour of the electric potential inside the medium satisfies the Laplace equation. It also allows for the field sources to be

specified explicitly (applicable if the source of the leak is known). To perform an inversion of SP and ERT data sets, the Newton least-squares method with regularization is used.

$$(A^T W^T W A + \mu C^T C)\Delta m = A^T W^T \Delta f - \mu C^T C m$$

Equation 1.6

Where A is the matrix of partial derivatives of measured values by section parameters (Jacobian), C is the smoothing operator, W is the matrix of relative measurement errors, m is the vector of required parameters, μ is the regularizing parameter, and Δf is the vector of discrepancies between the observed and calculated values. This process yields current distribution, which can be used to calculate seepage (Darcy) velocities (Zond, 2022).

2 Aims and Objectives

TerraDat UK Ltd. have been using geophysics to characterise earth embankment dams and detect potential preferential seepage pathways for several years. Their standard practice includes performing topographic surveys to identify features of interest and variations in topography which may be a sign of internal erosion. Ground conductivity and magnetic surveys are conducted over embankments to identify broad changes in ground conditions, usually relating to clay and moisture, and to identify ferrous features which may corelate with engineered structures. Usually, this is followed by several ERT surveys which are then presented as 2D pseudo-sections. Sometimes these pseudo-sections are presented as 3D fence diagrams to better illustrate continued features or variation between profiles. Occasionally, manual SP surveys are performed to identify areas of potential seepage flow at the time of the survey. These techniques are sometimes repeated at contrasting times of the year and at different reservoir levels to provide snapshots of how the hydraulic regime of earth embankment dams changes over time. Ground Penetrating Radar (GPR) surveys are often conducted over dam crests and inside spillways to identify areas of degradation.

A common observation in TerraDat UK Ltd.'s interpretation of ground conductivity and ERT data is the inability to explicitly define the nature of conductive zones (usually less than 100 Ωm). These more conductive areas are often attributed to increased clay and/or moisture content. It would be extremely valuable to be able to distinguish between these two sources of increased conductivity, especially when looking for areas of relatively increased moisture content linked with potential seepage pathways. Secondly, displaying ERT data as 3D contoured models would allow geophysicists and clients to better understand and visualise subsurface conditions at their sites.

Over the last few years, TerraDat UK Ltd. has been developing a remote SP monitoring system. This system is called SPiVolt. SPiVolt combines comprehensive background engineering geophysics with modern wireless technology to create a remote leakage monitoring system for the water industry. The system can display data in near real-time via an interactive web portal which clients can access securely.

The original version of the SPiVolt system consisted of 15 non-polarising electrodes connected to a data logger. The data logger was set to record the voltage of each sensor with respect to a common reference sensor every four hours, replicating a manual SP reconnaissance survey. TerraDat UK Ltd. aims to improve this system by enabling it to record other parameters such as temperature and battery percentage; increasing the number of sensors the system can support; and adding the ability to access the processed data remotely. The original SPiVolt system involved directly wiring each non-polarising electrode to the SPiVolt Hub manually. This method is complicated, hard to reproduce in the field, and leaves electrical connections somewhat exposed. The electrode and cable network design require refinement.

TerraDat UK Ltd. has since developed a bespoke "SPiVolt Hub," allowing for 64 channels; the remote download of data; improved battery life; and the ability to record temperature, reference temperature, air temperature, air pressure, and battery percentage. The system can upload data to a remote server, taking measurements approximately every twenty minutes. The system will last for three months on one battery charge in its current rendition.

Taking the above into consideration, the aims and objectives of this project were to:

1. **Characterise the study site using traditional TerraDat UK Ltd. methods.**

    a. Perform an electrical conductivity survey to characterise the top ~ 3 mBGL – 5 mBGL of the subsurface.

    b. Perform a magnetic survey to identify any buried ferrous objects which may give rise to conductive anomalies or indicate the presence of engineered structures.

    c. Perform an ERT survey consisting of ten profiles to characterise the study site at depth.

2. **Create a 3D resistivity model of the study site.**

    a. Perform a 3D inversion of the ten ERT profiles.

3. **Distinguish between moisture rich and clay rich zones at the study site.**

    a. Perform an IP survey and compute the normalised chargeability to delineate between bulk and surface conductivity effects; thus, determining the nature of more conductive areas.

4. **Create SPiVolt monitoring network and install a SPiVolt monitoring system at the study site.**

    a. Design a cable network which will integrate with the existing SPiVolt Hub.

    b. Design a cost-effective non-polarising electrode design and installation practice which will allow for stable and accurate measurements of SP fields.

    c. Install the SPiVolt monitoring network at the study site.

    d. Identify anomalous areas of subsurface flow linked to reservoir level and/or rainfall.

3 Study Site

A confidentiality agreement was signed prior to the completion of this project. As a result, the name, location, and some other details about the site have been redacted. Grid references have also been removed from figures. A review of available information of the site has been summarised in the form of an Initial Conceptual Site Model (see Section 3.8).

3.1 Site Description

The existing site layout is presented in Figure 3.1. The reservoir occupies one of a series of glacial cirques that form the northern escarpment of the regional coalfield uplands. The reservoir is impounded by an earth-fill embankment dam approximately 400 m long with a puddle clay core extending across the cirque. According to the dam zoning categories outlined in Foster et al. (1998), the dam is an example of a puddle clay core earth embankment dam. The dam was constructed in 1914 and rises approximately 20 m above the original ground level (as measured from the base of the downstream shoulder). The downstream shoulder comprises 'peat' excavated from the reservoir basin and fine material overlying the pre-existing geology. The embankment terminates at a rubble-stone toe.

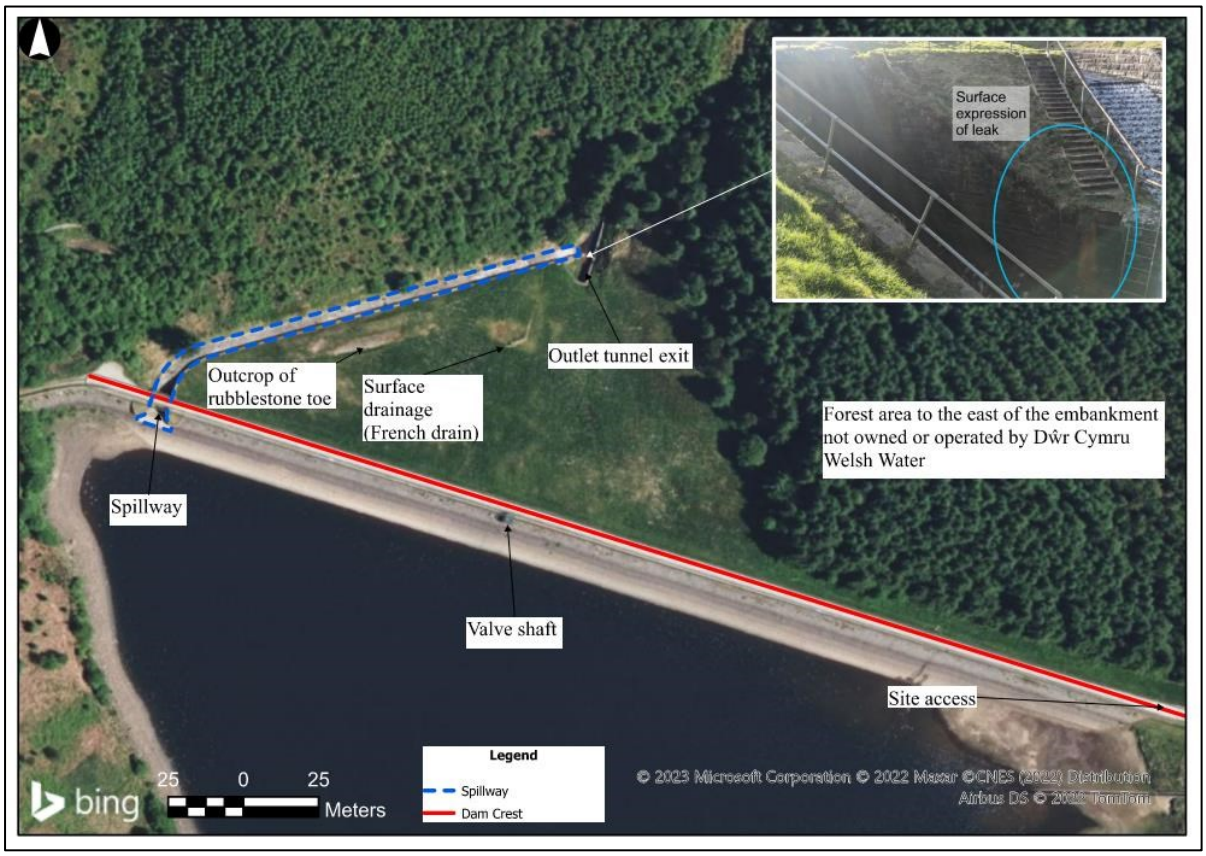

Figure 3.1: *Existing site layout.*

The downstream shoulder is grassed with large hummocks in some areas. The slope of the embankment is steep and irregular with topographic highs in the east and west, creating a subtle 'amphitheatre' shape (see Figure 3.2). The embankment is bounded by a spillway to the west and a forested area to the east.

Figure 3.2: Top: *Topographic relief across the downstream shoulder.* ***Bottom:*** *Photo of site conditions.*

3.2 Site Geology

The reservoir is underlain by coal measure formations comprising alternating beds of mudstone, siltstone and sandstone (UK Research and Innovation, 2020). A 1963 borehole log recorded by the British Geological Survey (BGS) is located close to the dam (location shown in Figure 3.3). The log shows mudstones were encountered between 3 mBGL and 14 mBGL, then 1 m of coal fragments overlying seat-earth which extends beyond the extent of the BH (16.3 mBGL). The bedrock geology strikes northwest to southeast (parallel to the dam crest) and dips at ~ 20º. The superficial deposits in the cirque are recorded by the BGS as diamicton (unsorted sediment with gravel in a fine mud matrix) and unsorted mud sediment. The latest Section 10 report from 2010 describes this as "boulder clay". The historical drawing references

'peat' extracted from the lakebed were used in construction. However, it is thought likely that materials accumulated within the cirque lake comprise a mixture of granular colluvial deposits, peat, silts, and mud. Figure 3.3 shows the published geology of the area, taken from the BGS GeoIndex.

Two borehole logs from 1963 are available via the BGS within the vicinity of the site. The location of these boreholes is shown on Figure 3.3; however, little certainty is given to their exact locations (the boreholes appear to have been drilled within the reservoir itself which is highly unlikely). Both boreholes are mapped as being drilled in the same location. The log confirms the presence of coal measures beneath the site comprising interbedded mudstone, siltstone, and sandstone.

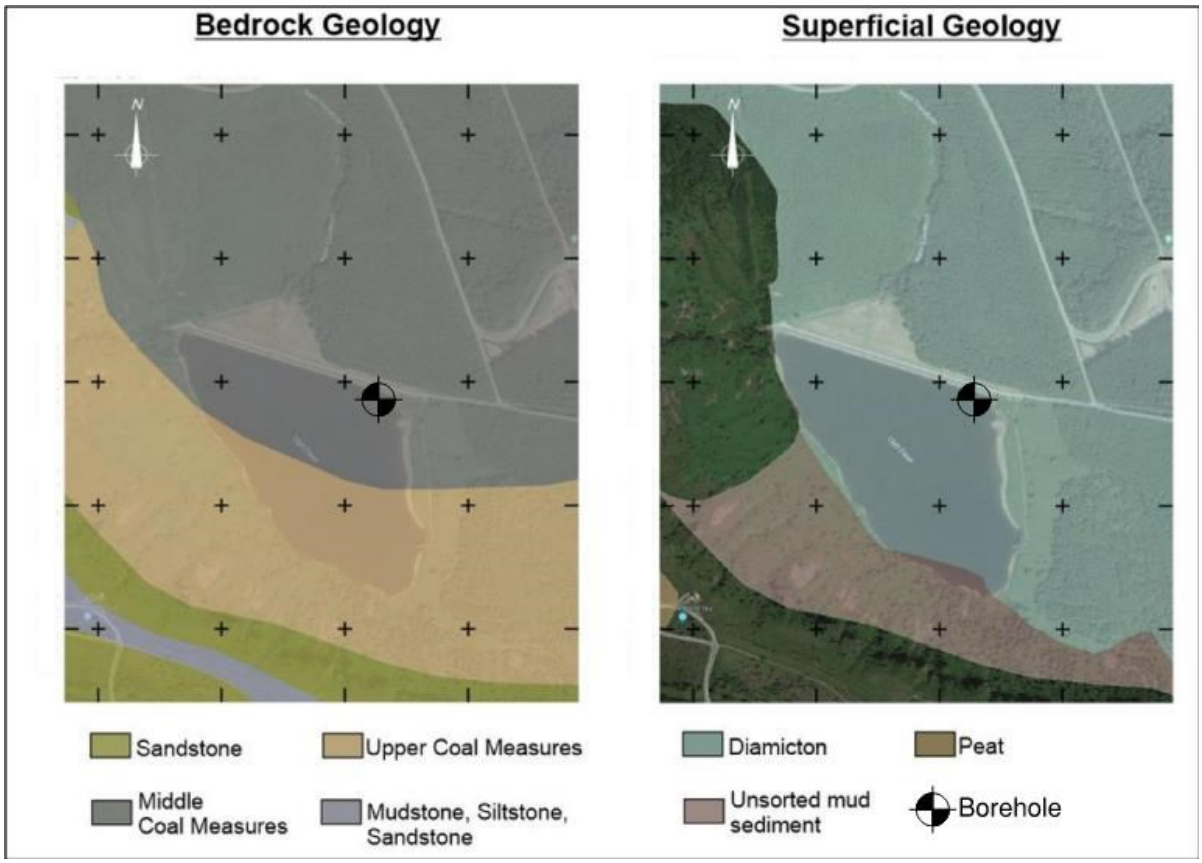

Figure 3.3: *Map of superficial geology as shown in the BGS GeoIndex* (UK Research and Innovation, 2020).

The expected stratigraphy beneath the site and anticipated thicknesses are presented in Table 3.1.

Table 3.1: *Expected stratigraphy beneath the site.*

Strata	Description	Thickness
Topsoil/Made Ground	Topsoil comprising the grassed area of the embankment. Made ground comprising compacted gravels to be present along the dam crest.	Topsoil – 0 m – 0.5 m Made ground 0.30 m – 0.5 m
Engineered Fines/Glacial Till	Clay rich sand and gravel.	~10 m at the top of the embankment near the crest, thinning to 0m at the dam's toe.
Coal Measures	Interbedded Mudstone Siltstone and Sandstone	Nearest borehole shows coal measure to continue for 60 m.

3.3 Mining

The study site is situated in an extensively mined area of South Wales. The Coal Authority's coal mining data was consulted to investigate the risk of encountering mining features such as shafts, adits, and workings beneath the site (Coal Authority, 2023). The nearest mine shaft/adit is situated ~ 1.2 km north-east of the study site. Figure 3.4 shows two coal outcrops to bisect the site west-to-east. The northern most of these outcrops bisects the study area.

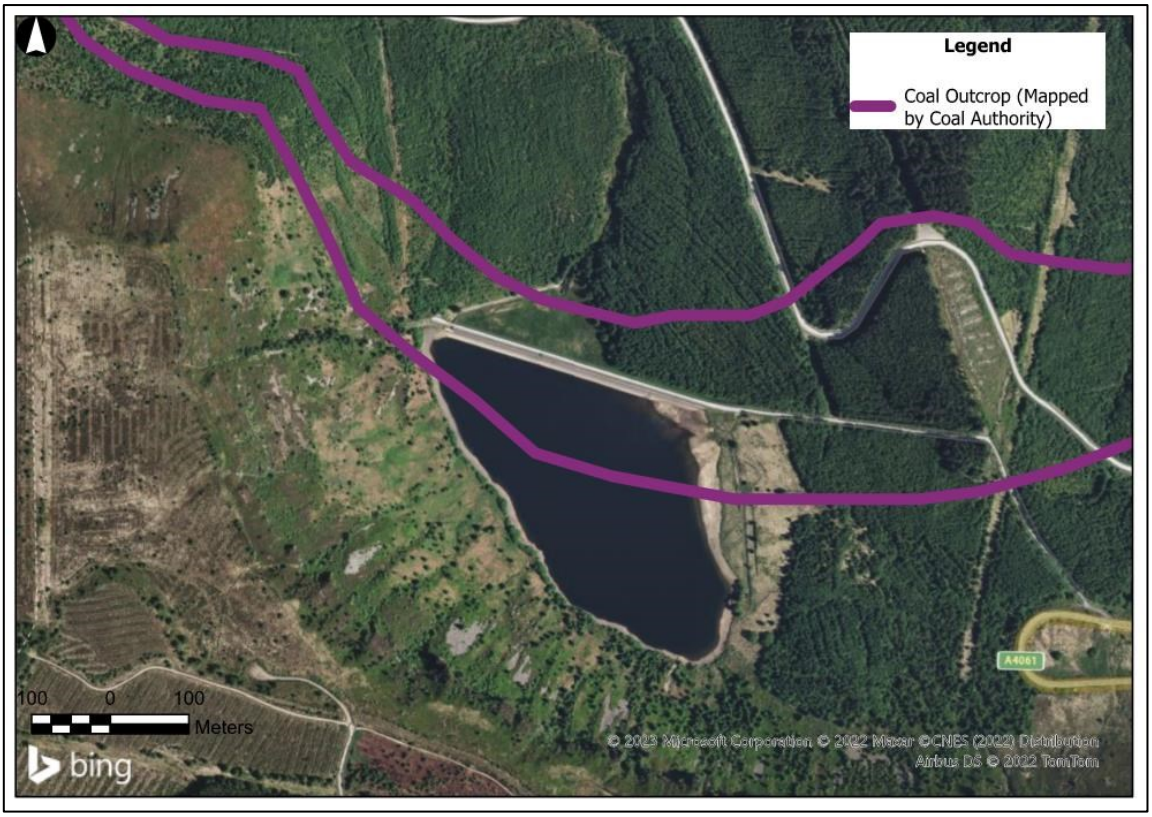

Figure 3.4: *Map of coal outcrops as mapped by The Coal Authority* (Coal Authority, 2023).

Records provided by Dŵr Cymru Welsh Water show that historical coal mining took place in the area surrounding the reservoir. In a letter dated 17th April 1967, there is a statement that "no workings have taken place in the Nine Feet and Four Feet workings that are likely to affect the reservoir". No new workings were contemplated at that time. A nearby colliery closed in 1994 but was bought by the miners and operated as a cooperative until the reserves were exhausted. It was eventually closed in 2008.

3.4 Catchment

The reservoir has a small direct catchment around its natural shoreline, whilst most of the yield is provided via a 1.8 km long tunnel that runs south to connect the reservoir to surrounding headwaters. The direct catchment area is given by the owners as 0.998 km^2 and is described as "very steep mountainous slopes draining part-forested moorland." The current 1:25,000 Ordnance Survey map indicates that the steep slopes along the southwest shoreline are unforested and rise to cliffs near the top of the escarpment, while the gentle slopes to the east and on the plateau above the escarpment are a mixture of moorland and afforested areas. Most of the direct catchment is defined as access land under the Country and Rights of Way Act 2000. The owners describe the indirect catchment area (upper valley) as "3.30 km^2 stream draining steep part-forested mountainous moorland."

3.5 Dam Details

A series of twenty drawings of the tunnel and reservoir (most of them unsigned and undated) were available to be consulted for this study. Most of them carry tender and/or contract numbers, ranging from 1906 to 1909. Although most drawings appear to show proposals rather than construction records, they are considered to mostly represent the works constructed. There are also several drawings (again mostly unsigned and undated) that show records of the construction work. One of the drawings contains a record of the puddle trench excavation profile, reaching a maximum depth of 21 m (70 ft). This drawing also shows the top profile of a concrete cut-off that was evidently placed at depth, presumably to limit the variation in the depth of the puddle clay core beneath the original ground level. Over most of the dam length, this is in the range of 6 m to 9 m, with a maximum that can be scaled as about 11 m. The concrete cut-off extends to above the culvert, and a concrete pillar down through the cut-off trench supports the spillway channel where it crosses the core.

The deepest section of the cut-off excavation is at the left (west) abutment, where it continues for approximately 100 m beyond the apparent end of the dam and is partially sunk below a "drift." In this area, the cut-off trench is shown filled with concrete to 1 m (3 ft) above the overflow level.

Over most of the length of the dam, the cut-off trench terminates in boulder clay (glacial till), with "rock" and a "2 ft good fireclay" seam exposed in the extension of the cut-off beyond the left abutment and shale beyond the right (east) abutment. Another drawing shows a longitudinal section of the cut-off trench, including the encountered stratigraphy. Another drawing includes information on excavation dates, indicating that work started in 1909 and that the trench was bottomed out in the summer of 1910.

Another drawing shows peat excavation progress, with a total volume of almost 95,000 (units not given, but presumably cubic yards). This drawing contains a graph showing monthly volumes between June 1909 and March 1912, rather than the geographical locations of peat removal or disposal. The above volume of peat is only about 40% of the volume of 25,000

cubic yards noted previously. Therefore, it appears that peat excavation must have continued after March 1912.

Another drawing of circa 1906-1909 shows a large spoil bank overlying the downstream shoulder, clearly where the peat would have been deposited. In this section, the cross-sectional area is approximately 600 ft^2. This is comparable with disposing of the quoted volume of 25,000 cubic yards in the raised dam shoulder.

A 1921 drawing shows a dam plan with a downstream slope of 1 in 2.5, that is, with no spoil bank of peat shown. The spoil bank was likely omitted only to show the "engineered" structure.

The reservoir is impounded by an earth-fill embankment dam approximately 400 m long, with a puddle clay core, across the natural valley. The dam crest is approximately 400 m long, with a maximum height above the original ground at the downstream toe of the order of 20 m. It is orientated on a straight line of bearing of 107° to the national grid, with a concave upstream curve at the left abutment. According to the dam break report, the overall embankment comprises two dams, of which the western dam is short and closes off a subsidiary valley. However, this interpretation is not borne out by historical drawings, which clearly indicate a continuous embankment and cut-off along the entire length (albeit with a short interruption to the embankment at the overflow structure).

Drawings from around the time of construction show a 4.5 m wide dam crest and an upstream face that is protected by stone pitching, generally sloping at 1 in 3, but curving upwards near the crest to form a 0.6 m high masonry wave wall. The present wave wall is concrete, so it is assumed that the decision to change the form of the wave wall was made at the time of construction.

The downstream shoulder of the embankment slopes at 1 in 25, but the surface is very irregular. The gradient is gentler where it is overlain by copious quantities of "peat" excavated from the reservoir basin at the time of construction. The dam has a puddle clay core, which continues down into a cut-off trench, but historical drawings of the cut-off works show that the lower part of the trench was filled with concrete. The shoulder fill is shown as inner and outer zones, with the inner zone being labelled as "fine material." Historical drawings also indicate that the upstream toe of the dam was terminated in a concrete retaining wall, and the downstream toe of the peat spoil bank was terminated in a "rubble-stone toe."

The overflow comprises a curved masonry weir of nominal length 6.7 m located near the left abutment of the dam but found original ground. This discharges via a series of steps into a short-arched culvert, 5.49 m wide and 2.48 m high beneath the dam crest. Historical drawings show the culvert foundation connected with a concrete-filled section of the cut-off trench directly beneath it. Downstream of the culvert, the spillway curves by approximately 60° to the right and then runs in a straight line along the outside of the left mitre of the dam, which in this area is substantially extended by the peat soil bank, for approximately 120 m before curving left and descending via a series of steps (1 in 2) to join the channel downstream of the draw-off tunnel. The spillway gradually reduces in width, from 5.48 m at the culvert to 4.11 m at the downstream end of the curve and to 3.05 m at the downstream end. The initial gradient is shown as 1 in 20, then steepening to 1 in 6 and then levelling off to 1 in 25 before the steps. The spillway construction is shown as a 1 ft thick masonry floor bedded on 1 ft of concrete and the walls as masonry backed with concrete, again with a total thickness of 2 ft.

There is a combined 560 mm inlet and outlet pipe laid within the tunnel that links the reservoir to the adjacent valley. At the northern end of the reservoir, the tunnel slopes initially downwards at a gradient of 1 in 2 with two intermediate landings for approximately 100 m. It originally ran at a gradient of 1 in 600 downwards to the southern portal, but subsequent mining subsidence has resulted in the tunnel profiling having "sag," so now requires pumped drainage. The northern steeply sloping section of the tunnel includes connections to the reservoir at three levels, with the pipes having their centreline levels approximately 4.5 m, 9 m, and 13.5 m below the reservoir overflow level (based on historical scale drawings). Historical drawings show the outlet tunnel from the reservoir, which passes beneath the dam slightly towards the left of the dam centre, together with a dry-well valve shaft, about 20 m deep, located against the upstream side of the puddle-clay core. This tunnel served as the drainage rout from the basin of the natural lake during the construction of the reservoir. An inspection report from 1970 describes the reservoir's draw-off works: The valve shaft in the upstream shoulder of the embankment communicates on the downstream side with a tunnel through a triangular-shaped brickwork "arch." From the drawings, this arrangement was designed for the diversion of water during construction and that it was intended to complete the brickwork to form a stop or bulkhead. This has never been done, and there is direct access from the shaft to the tunnel. In the same drawing, a tunnel or culvert constructed in cut-and-cover is shown on the upstream side of the shaft. The drawing shows dotted lines, presumably the outlines of an excavation, dated various months in 1910; cross-sections showing the cut-and-cover tunnel upstream have been deleted in pencil, and another drawing shows and 18-inch pipe in place of the culvert. There are no dates, or any other indication of which drawing is correct, but it seems more likely that the second drawing showing the pipe is correct. A geological section along the puddle trench shows boulders, ballast, and silt in this area to be very wet, suggesting that, after constructing the downstream section of the tunnel as far as the valve shaft, the construction then ran into difficulties and that the design was changed to the simpler pipe. No historical drawings show the construction method on the upstream side of the shaft. However, the geological cross-section contains the same soil description in the vicinity of the draw-off tunnel. In the past, there was a 150 mm supply main through the tunnel. The use of this was abandoned many years ago, although the pipe remains.

At the base of the outlet shaft described above, there are two in-line valves on the 610 mm scour pipe. Following recommendations from the 1991 report, these can be operated from the top of the shaft using a portable hydraulic actuator. The scour pipe is approximately 8 m long, starting at the bell mouth at the upstream face of the plug and discharging into the tunnel just downstream of the shaft.

Current monitoring instrumentation at the reservoir comprises:

- Facilities for monitoring water levels.
- Seventeen points along the dam crest for monitoring possible settlement.
- Four v-notch gauges for monitoring drainage/leakage flows downstream of the dam.
- Six piezometers in the downstream shoulder, of which only three have been read in recent years.

The water level is measured "manually by tape." However, gauge boards are located near the valve shaft and near the overflow. In addition, there is now a level sensor (pressure transducer) alongside the valve shaft, with remote monitoring facilities.

There is vehicular access to the right (east) abutment of the dam along a single-track gravel road, over approximately 600 m from the main road. There are turning and car parking spaces at each end of the dam. The downstream of the reservoir runs northwards through woodland for approximately 2 km.

3.6 Details of Modifications, Remedial Works, and History

Details of the dam's history acquired from Dŵr Cymru Welsh Water are presented in Table 3.1.

Table 3.1: *Details of modifications, remedial works, and History.*

Date	Summary of Incidents, Investigations, and Remedial Works
1896	An Act of 1896 conferred various powers, including converting the original corrie into a reservoir and driving a tunnel between the lake and the nearby valley.
1897	A series of drawings gave early proposals for the reservoir and tunnel. The reservoir level was to be raised by 7.6 m (25 ft) from 361 mAOD (1183 ftAOD) to 368 mAOD (1208 ftAOD) with an overflow at the right abutment.
1903	The local council decided to contact an expert water Engineer to consult on the project. It is noted that the engineer advised proceeding with an alternative scheme from the original proposed after careful consideration and discussion in their report.
1906	Tunnel driving commenced.
1909	Tunnel driving completed. Works on the reservoir commenced.
1914	Works on the reservoir completed.
1928	Mining starts to affect the reservoir and tunnel.
1933	Finished reservoir was reported to have a capacity of 200×10^6 gallons, a surface area of 25 acres, and a maximum depth of 21.3 m. However, an inferred maximum depth of 17.7 m (based on the difference between the original depth and the amount by which the lake was raised) is more consistent with information in historical drawings. Although this difference may be attributed to peat removal from the bottom of the reservoir basin, this appears unlikely, as there is no compelling reason to remove peat below the intake level to the scour and outlet pipes. Therefore, it can be conclude that the maximum depth of the reservoir is approximately 18 m.
1934	Dam inspection. Report not available.
1943	Dam inspection. Report not available. Most of the embankment had settled by about 6 inches up to 1943 (according to 1953 report).
1953	Dam inspection. • No change in embankment settlement since 1943. • It was mentioned that the embankment was built on coal measures "which is likely to be worked on in the near future. Steps should be taken to prevent the working of sufficient area of various seams of coal to ensure that no subsidence takes place." The reservoir was considered to be "safe and well maintained" but warned that "should coal be worked underneath, and any movement be observed, a report should be called for immediately."
1958	The original supply main was replaced due to subsidence damage (according to 1994 report).
1963	Dam inspection. Report not available. Was noted that "The top coal seam has been worked some little distance away from the top water line of the reservoir along both sides, but that on the Western Side

	seems to undermine the end of the concrete core of the embankment, which was carried into the hillside of a distance of about 230ft." It was noted that "in conjunction with the National Coal Board, which is checking the levels, is reported at three monthly intervals" and that "there has been slight movement in the top level of the wave wall of the embankment on which the levels are taken." The report warned "If any greater movement takes place, it must be considered very serious," and "Any movement by mining, which would allow percolation of water, would be disastrous with the collapse of the embankment probably in a matter of hours". It was recommended "Other coal seams should not be worked below the reservoir embankment as it may disturb the pillars in the 9 ft seam." (According to 1994 report).
1967	It was summarised in a report that the impact of the coal workings from collieries on the reservoir that "no workings have taken place calculated to affect reservoir" and "non are contemplated." Levels were taken on a series of rivets along the top of the wave wall and revealed a maximum settlement in eight years since 1959 of 21 mm. It was recommended to continue level monitoring, installing leakage gauges at the downstream end of the reservoir draw-off tunnel and at the foot of the retaining wall at the left mitre and an interval of three years to the next inspection.
1968	Installation of leakage gauges at the downstream end of the reservoir draw-off tunnel and at the foot of the retaining wall at the left mitre,
1970	Dam inspection. • Noted that deposition of "about one-inch depth of clayey material beneath the outlet scour pipe." • It was reported that "No settlement or movement of the embankment which might affect the stability of the reservoir is at present apparent. However, in view of the extent to which the dam has already been undermined in the Nine Feet Seam, the approach of workings in the replacement seam must be considered a serious threat to the stability of the dam if the workings approach nearer than a line giving an angle of draw of 45° from the upstream toe of the dam." • Concerning potential movement of the land surrounding the reservoir, "An examination of the area around the reservoir has been conducted to assess the possibility of large rock falls from the cliffs which partially surround the reservoir and rise to a hight of 550ft to 650ft above it." "Degradation takes place, in general by mechanical weathering along relatively closely spaced joint and bedding planes to form scree slopes. Rockfalls have taken place at some time in the past over a limited area but have involved only small quantities of material. There is no evidence of the formation of cracks on the plateau behind the clifftop. The likelihood of a fall of rock being large enough to have disastrous consequences is considered remote." • It was noted that there was some vertical displacement along the wave wall at the valve shaft and spillway. The access had to be improved, with turning space provided at each end of the dam.
1975	According to a report on instrument readings, the six piezometers "have all remained steady over the period July 1973 to February 1975, with very little change due to either season or the reservoir level". It could be concluded that the puddle clay core "is shown to be watertight in relation to the downstream shoulder."
1976	Dam inspection.

	• It was noted that an additional gauging weir had been installed "to measure seepage appearing in the tunnel portal." No further mining had taken place near the reservoir since 1970.
1980	Dam inspection. • Concerning clay deposits in the reservoir tunnel, the report noted, "After the last inspection, five deposits from the tunnel floor and walls were analysed in relation to a reference sample from the embankment core. Details are given in separate correspondence, but the results show no evidence to connect the tunnel deposits with the dam or the surrounding ground." Records from five piezometers were examined, and "levels generally responded closely to reservoir level. No recommendations were made that were explicitly "in the interest of safety," but called for continual efforts on maintenance and monitoring fronts.
1985	Dam inspection. • It was reported that all the recommendations in the previous inspection report had been conducted. One recommendation was made in the interest of safety; "repointing of the defective pointing in the spillway channel and re-setting of the disturbed coping stones on its western wall should be carried out within the next twelve months to prevent further deterioration."
1994	Dam inspection. Advice was given on measures "to rectify deficiencies in the tunnel lining and alleviate flooding in the tunnel where these arise from mining subsidence." This concerned the tunnel linking the reservoir to the adjacent valley, so it did not relate directly to the safety of the reservoir.
2000	Dam inspection. • "The surface drainage system in the wet area on the downstream face should be improved." • "The small leak through the crest of the overflow weir should be sealed before it becomes any larger, and repairs to the joints in the masonry invert and walls of the spillway channel should be carried out from time to time; as necessary." • "The progressive frost damage to the wave wall should be made good within the next few years, and any damage to the pitching on the upstream face made good from time to time." • "The means of egress from the scour tunnel should be improved" (this is related to personnel access to the downstream portal of the draw-off tunnel).
2003	The Supervising Engineer's annual statement notes that a "small slip" occurred on the scree slope above the reservoir.
2009	In November, conifers near the left mitre of the dam were felled, apparently causing an effect on local drain flows.

3.7 Details of the Most Recent Section 10 Report and Current Condition of the Site

According to the Section 10 Report conducted under the Reservoirs Act 1975 in March 2011 (the most recent inspection report available), the catchment remains widely unchanged. The indirect catchment was not inspected as it was considered not material to the safety of the reservoir.

The stone pitching of the dam's upstream face was considered in excellent condition where visible. However, the Supervising Engineer did note that the waterline suggested evidence of settlement at lower water levels. It was noted that a natural consequence of the "peat" surface on the downstream shoulder is that it tends to retain water and support reedy areas. In 2009, the dam's downstream face to the left of the overflow works was cleared of forestry trees. An area of ponded water was noted approximately 2 m below the dam crest level. This ponded water was found at a higher level than the water level in the reservoir, suggesting the source must have been surface run-off from the dam.

Overall, the overflow works were considered "fit for purpose." The valve shaft and tunnel were in "sound condition." At the time of inspection, it was noted that some seepage emerges from the steps of the overflow works when the water in the reservoir is high. Three locations with concentrated seepage into the tunnel were noted. However, these were of "no concern at present." The inlet and outlet pipework and valves were not inspected on the grounds that any failure or malfunction of the pipework would not pose a significant threat to the reservoir.

The Section 10 Report contains an examination of v-notch readings for the period 2000 – 2010. Three v-notch locations outlined below were examined. Daily rainfall and reservoir levels were also examined for most of the years.

- **Western Toe:** Downstream of the retaining wall that forms part of the dam located near the left abutment, beyond the overflow works.
- **New Embankment:** Located in a chamber alongside the right side of the spillway just upstream of the point where the spillway steps down to join the tail bay channel downstream of the tunnel portal.
- **Tunnel:** Picking up leakage into the shaft and tunnel

Water flow through the west toe remained constant between 2000 and 2009, but the maximum flow doubled in 2010 following the felling of trees in this area. However, following reports produced post-2010, it was speculated that the leakage past the gauge was reduced by an accumulation of debris sealing former leakage pathways. It was suggested that further monitoring should occur to determine whether there had been a permanent change or whether there was a progressive return of the previous flow rate.

The readings from the new embankment clearly showed a response to rainfall. This was expected because of its location towards the downstream edge of the "peat" overlying the downstream shoulder of the dam. Flows through the tunnel showed less variation, which suggested a deeper seepage or leakage pathway.

Currently, only three piezometers are present at the site. These are noted as P3, P4, and P5 (locations of these piezometers can be seen in Figure 5.1). It was concluded that all three piezometers in the downstream shoulder remained at acceptable levels during the monitoring period 2000 – 2010. During this inspection, there was no evidence of any untoward seepage from the embankment. The report also concluded that the amount of settlement along the dam's crest was within the range of an embankment dam of this age.

In 2021, the reservoir owner was tasked with conducting a seepage investigation to identify potential preferential seepage pathways through the dam, which may be linked to seepage observed at the location identified in the Section 10 Report. The owner tasked an external

contractor with conducting an active geophysical leak detection survey to map possible preferential seepage pathways. The method used involves introducing an alternating electrical current at a specific frequency directly through the water (the reservoir and at the leak) to establish an electrical current. Earthen materials enhance the electrical conductivity of the water, with current using the preferential seepage pathway as a path of least resistance to complete the circuit. Magnetic highs can then be detected at the surface through a bespoke magnetometry survey. The magnetic field can then be analysed to reveal the locations and depths of potential preferential seepage pathways. This survey identified two preferential seepage pathways.

Although current follows the path of least resistance, this cannot always be attributed to preferential seepage pathways. For example, Reynolds (2011) notes that rainfall-runoff (analogous to freshwater found in the reservoir) can be expected to have a resistivity of 20 Ωm - 100 Ωm. Measurements of the resistivity of materials such as sandstones fall within the range of 1.0×10^{8} Ωm - 7.4×10^{8} Ωm, which contrasts highly with rainfall-runoff. However, materials such as clay and boulder clay (materials that are often used in the construction of earth embankment dams) have resistivity values of 1 Ωm -100 Ωm and 15 Ωm - 35 Ωm, respectively. Therefore, in these situations, the path of least resistance cannot necessarily be attributed to the preferential seepage pathway through an earth embankment dam. Secondly, one preferential seepage pathway seems to run parallel to the dam's crest and the boundary fence of the forested area to the north. Such a sizeable metallic feature would influence the results of a magnetometry survey. However, there is no mention of the effect of this metallic body in the report. The effect of the fence on both ground conductivity and magnetometry surveys conducted for this project is clear to see and is accounted for in Section 5. Thirdly, magnetic data is compared to a homogeneous model of surface conductivity to identify preferential seepage pathways. As this thesis explains in Section 5, the downstream shoulder of the embankment is far from uniform, with resistivity (inverse of conductivity) values varying by several orders of magnitude.

3.8 Initial Conceptual Site Model

Figure 3.5 shows two schematic cross-sections digitised from a series of historical drawings. It should be noted that the georeferencing and scaling of these cross-sections can only be estimated and are thought to be correct within +/- 5 m on the x-axis and +/- 2.5 m on the y-axis

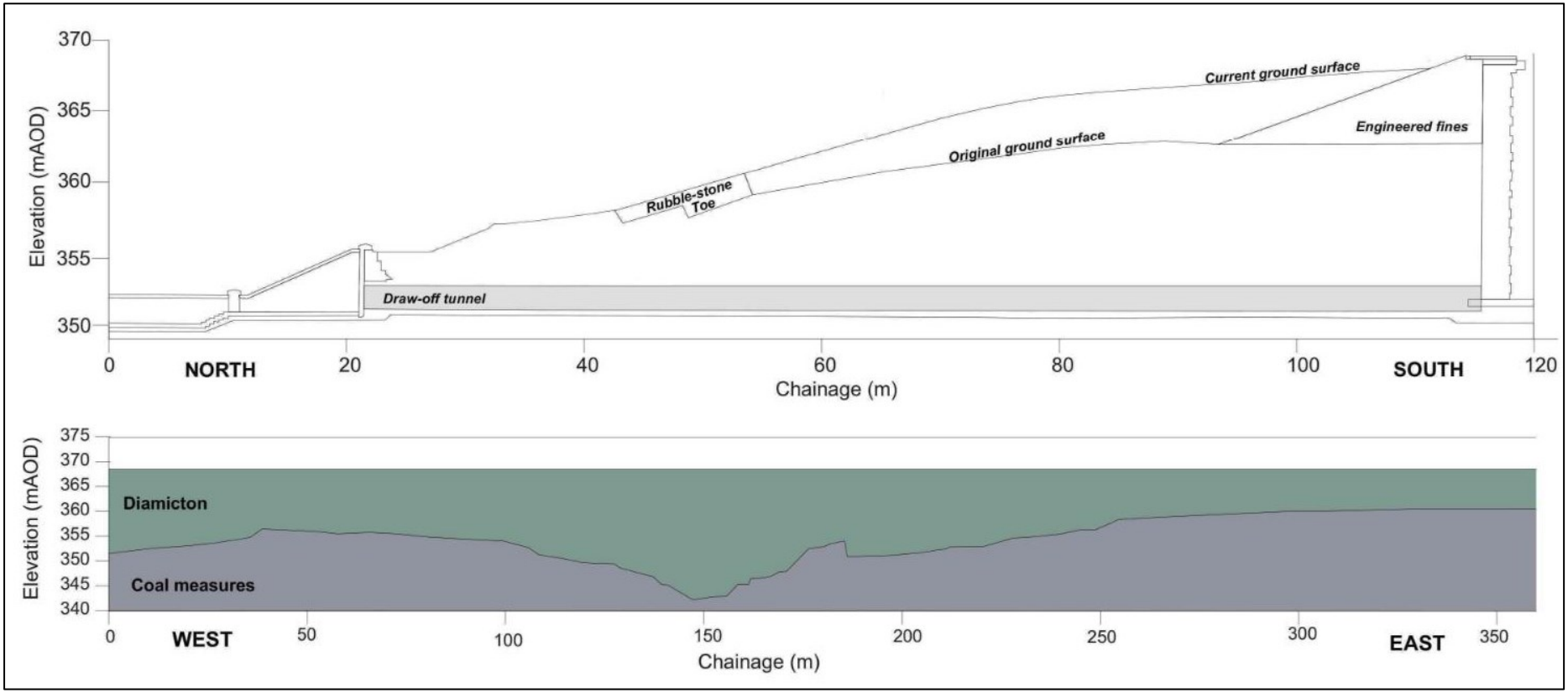

Figure 3.5: Top: *Initial conceptual cross section perpendicular cross section to the crest of the dam.* ***Bottom:*** *Indicative cross section along the crest of the dam, taken from historical drawings at the time the dams construction.*

4 Methodology

4.1 Dam Characterisation Survey

The geophysical data were collected in line with normal operating procedures outlined by the relevant instrument manufacturers and TerraDat UK Ltd.'s company policy. Upon completing a survey, the data was downloaded from the survey instrument onto a computer and backed up appropriately. Acquired datasets were initially checked for errors that may be caused by instrument noise, low batteries, positional discrepancies, etc., and any field notes were either written up or incorporated in the initial data processing stage. Datasets were then processed using standard processing routines. Quality control standards were in accordance with BS EN ISO 9001: 2015. The location of each technique deployed is presented on a subplot on each figure.

The characterisation survey was conducted using ground conductivity, magnetometry, ERT and IP techniques. The results are presented in the form of data plans and cross-sections, indicating the location and physical characteristics of identified anomalous features together with text descriptions.

A Topcon Hiper+ RTK GPS was used to survey the positions of the piezometers and other features. Topographic points and key features were recorded and subsequently combined with a site plan provided by Dŵr Cymru Welsh Water. The location of the ERT and IP electrodes were also surveyed using this instrument. The ground conductivity and magnetometry data was acquired using 2 m spaced survey lines under the positional control of an EGNOS corrected dGPS.

4.2 Self-Potential (SP) Monitoring Network

The SPiVolt monitoring array aims to replicate the process of performing a manual potential amplitude survey. The reference electrode must remain fixed, and fixed electrodes must replace the roaming electrode at each predetermined measurement location. The TerraDat UK Ltd. SPiVolt Hub is designed to be connected to nine ethernet cables. Ethernet cables contain eight individual channels; thus, each cable is designed to be connected to eight sensors (with the ninth cable being used to connect the reference electrode and other sensors) (Figure 4.1). Measurements are taken by the SPiVolt Hub, recorded internally, and assigned at UTC timestamp. These observations are stored locally as separate CSV files before being uploaded to a remote server through the strongest phone network using a multi-sim. The data is then compiled into one continual CSV file which is accessed using Python through a bespoke Application Programming Interface (API). The downloaded data is then formatted and converted into a Pandas Data Frame within Python for processing. A second API is then used to upload this data, allowing it to be displayed appropriately on the SPiVolt website (https://www.spivolt.net/).

4.2.1 Non-Polarising Electrodes

The design of the non-polarising electrodes is based on the second generation of lead-lead chloride electrodes for geophysical applications developed in Petiau (2000). The final design of the copper-copper sulphate electrodes developed for this project can be seen in Figure 4.2. Firstly, 300 mm long sections of push-fit PVC-U waste-water tubing (32 mm diameter) were cut using a bench saw, and the edges sanded. 2 cm disks of 32 mm wide wooden dowl were cut using the bench saw and secured into the end of the tubing. The inside of the tubing was scored with sandpaper, and a small amount of bathroom sealant was applied to secure the

porous wooden plug. A protective plastic cap and rubber bung were attached to each stranded cable section as part of the network design. This allowed for easy deployment in the field. A neoprene washer was inserted into the bottom of the tube, flush with the porous wooden plug. This aimed to reduce the rate at which the copper sulphate solution seeps through the porous plug by reducing its contact area, prolonging the longevity of each electrode.

Figure 4.1: *Photograph of inside the SPiVolt Hub.*

Each electrode was filled with a solution of copper sulphate, water, glycerine, and bentonite at a 1:1:1:1 ratio. Boiling water was used, and all the solution elements were mixed thoroughly by shaking them in a container for approximately five minutes. Glycerine was added as an 'anti-freeze' for the electrolyte solution. A protective cap was then attached to the top and bottom of each electrode, and they were stored upright in a bucket to prevent any solution from spilling out.

4.2.2 Continuous Network Cables

A continuous network design is analogous to performing a manual potential amplitude survey, as a direct wire links the reference and measurement electrodes to the voltmeter (SPiVolt Hub). Fewer connections should yield less noise within the data. However, cable networks can only be made at discrete lengths, and alterations or repairs to the network in the field may be complex. Figure 4.3 shows each stage of fabrication of the continuous network cables.

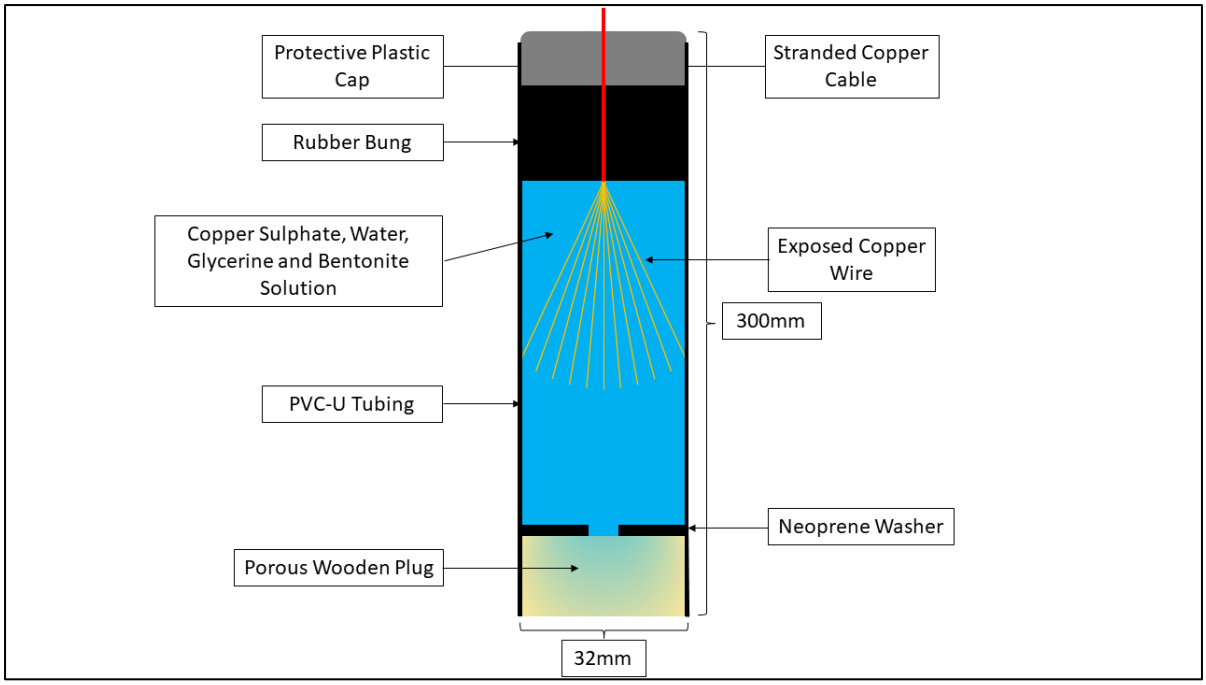

Figure 4.2: *Cross-section of copper-copper sulphate electrode used for the project.*

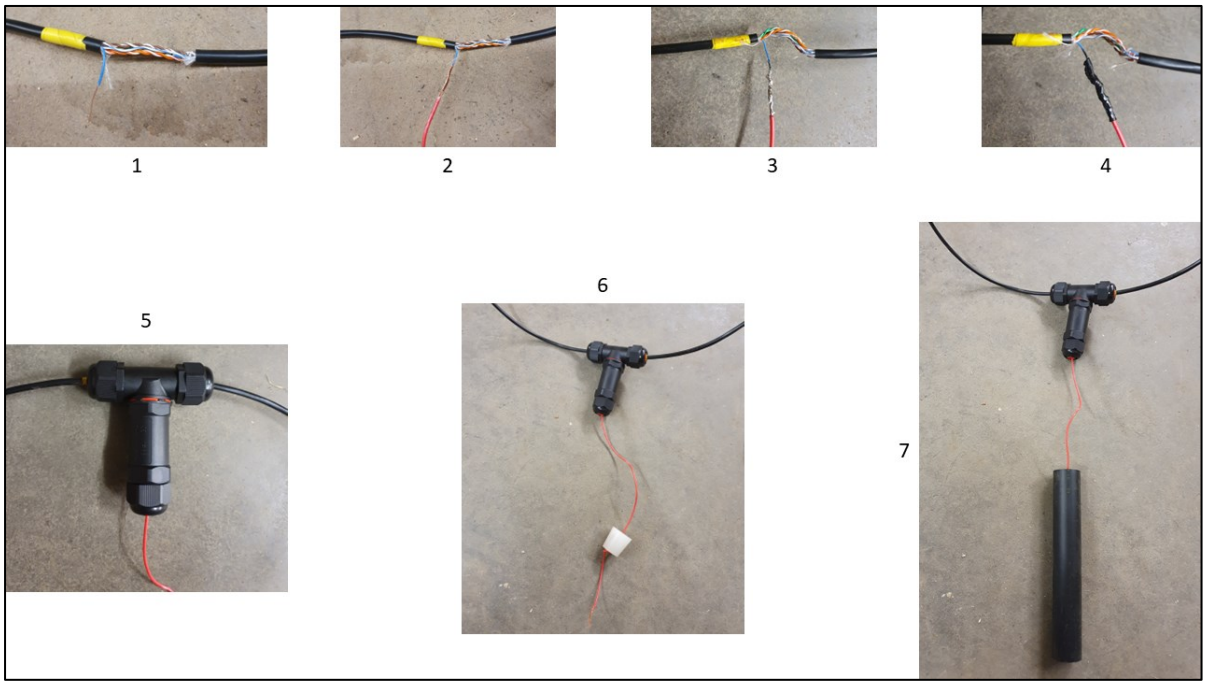

Figure 4.3: *Each stage of continual network fabrication.* ***1.*** *Removal of the outer sheath of ethernet cable.* ***2.*** *Removal of the outer sheath of the stranded copper cable.* ***3.*** *Stranded copper cable soldered to individual ethernet channels.* ***4.*** *Wrapping the solder joint in a heat-shrink wrap to protect the solder joint.* ***5.*** *Encasing connection in an IP68 certified waterproof housing.* ***6.*** *Attaching rubber bung to stranded copper cable.* ***7.*** *Connecting wire to the non-polarising electrode.*

4.2.3 Installation

A 64 channel SPiVolt system was installed into the embankment between the 7th and 15th March 2022. The locations of sensors were determined after analysing the results of the characterisation survey. The layout of the array is shown in Figure 4.4.

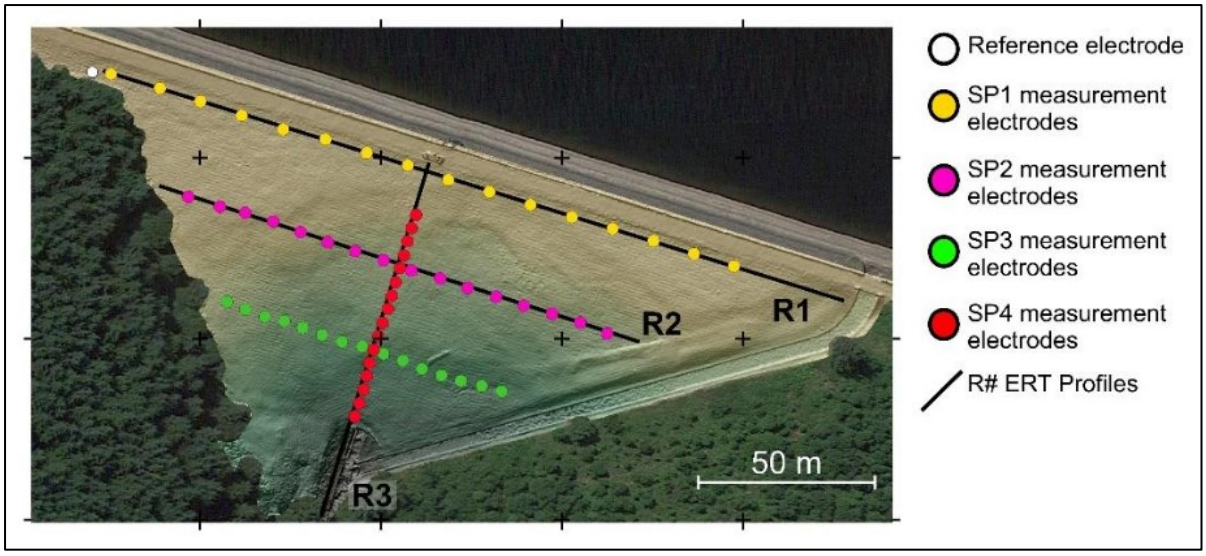

Figure 4.4: *Location of SPiVolt electrodes.*

It was important that the cables were buried to avoid being eaten by fauna or being tampered with by members of the public. Burying these cables purely by hand would be extremely labour intensive and take a very long time. To make this process more efficient, a "lawn edger" was re-purposed for cutting a small narrow trench in the ground which the cables could be fed into (Figure 4.5). Normally, these machines are used to trim the edges of lawns for residential properties. They consist of a small two-stroke petrol engine which is connected via a belt drive to a cutting blade. The cutting blade was adapted by installing two sharpened cutting blades separated by a ~ 3 cm washer to enable the edger to break through matted roots and create a narrow trench. The result of this process is shown in Figure 4.6.

Holes for the non-polarising electrodes were created by using a wooden pole with a diameter slightly wider than the electrode's and hammered in using a mallet. These were created at a consistent depth via placing a tape marker on the wooden pole. These holes were then filled with bentonite to reduce the rate of seepage of the electrolyte into the ground.

All electrodes were connected back to the SPiVolt Hub through a secure cable management speed bump, which was drilled into the hardstanding track at the crest of the embankment to prevent damage from vehicles. These cables were then fed through a section of plastic tubing into the secure valve cage to prevent damage from members of the public (Figure 4.7). These cables were then colour coded and connected to the SPiVolt Hub to allow for easy maintenance in the future. The SPiVolt Hub, and its power supply, were sealed within a modified weatherproof case and wrapped in a tarpaulin (Figure 4.8). The SPiVolt system was then programmed to take a full set of measurements at 17-minute intervals and upload this data to a server every hour.

Figure 4.5: *Photograph of adapted lawn edger used for cutting trenches at the study site.*

Figure 4.6: *Photograph of trench cut using adapted lawn edger.*

Figure 4.7: *Photograph showing SPiVolt cables feeding through speed bump and plastic tubing into valve cage.*

Figure 4.8: *Photograph of SPiVolt Hub, power supply and cables secure in weatherproof case with valve cage.*

5 Results and Interpretation

5.1 Ground Conductivity

The results of the ground conductivity survey are presented in Figure 5.1 as a colour-contoured plot of ground conductivity (units mS/m). A reversed rainbow colour scale has been applied to allow comparison with ERT results; low conductivity (high resistivity) is coloured red, and high conductivity (low resistivity) is coloured blue.

In general terms, a localised increase in conductivity values usually indicates a relative increase in clay content or groundwater saturation of the shallow subsurface. Exceptionally low values indicate shallow resistive materials such as moisture deficient sands/gravels or many types of competent bedrock. Extreme fluctuations in the conductivity values are indicative of instrument 'overload' due to interference from nearby metal structures/debris. Ground conductivity surveys conducted with the GEM-2 instrument can identify features up to a maximum depth of ~ 3 mBGL - 4 mBGL.

The embankment is generally characterised by conductivity values of between 5 mS/m - 11 mS/m, which correlate with clay deficient engineering materials and diamicton as well as mudstones present within coal measure formations and is consistent with the geological mapping and historical cross-sections. Across the northern and north-western sides of the embankment, the dam is characterised by low conductivity (C1), suggesting the ground is dry and/or clay deficient. This zone is consistent with the location of the rubble-stone toe structure suggested by the historical drawings. Within area C1 is a localised area of increased conductivity (C2). This is an area of increased clay and/or moisture content and could be related to surface seepage noted in the most recent Section 10 Report. A broad zone of higher conductivity material on the eastern side of the embankment is evident (C3). This is likely attributed to an increase in clay content within the shallow subsurface or an increase in moisture content.

Ground conductivity data collected over the eastern access road is dominated by extreme high and low values (C4a) due to 'instrument overload' caused by the presence of shallow or surface metal; specifically, a wire fence along the northern side of the road. The southern side of the access road is dominated by low values, these can be attributed to hard engineered materials (e.g., gravel and concrete) used to construct the road that runs along the crest. Features C4b and C4c are also incidences of surface metal causing instrument overload. C4b is attributed to vehicles and the metal valve cage present along the crest of the dam. C4c is attributed to a metal railing which runs along the outlet tunnel. It is not possible to comment on the ground conductivity in these areas.

5.2 Magnetometry

The results of the magnetic survey are presented as the vertical gradient of the total magnetic field as recorded at two sensors positioned vertically, 1 m apart. Gradiometer surveys enhance small, shallow magnetic anomalies and can suppress broad regional changes, making them particularly useful in geologically or structurally complex locations; they are ideal where targets may be subtle and shallow. The interpretation of a magnetic anomaly is based on observing the type (monopole/dipole), amplitude and wavelength of the anomalous feature.

The magnetic survey was primarily conducted to advise on the location of any buried ferrous material, utilities, or structures across the dam, as these features would affect the SPiVolt monitoring array data. The effect of ferrous materials of piezometers P3 and P4 can be seen

clearly as negative monopoles due to their narrow cylindrical, vertical nature. There are numerous small monopoles and dipoles randomly distributed across the site. These are likely attributed to small ferrous debris and not related to remnant structures.

5.3 Electrical Resistivity Tomography (ERT)

The results of the surveys are presented in Figures 5.2 – 5.5 as colour-contoured, scaled sections of the subsurface showing changes in resistivity. The data is presented using a 'rainbow' colour scale, with blue representing lower resistivity (higher conductivity) and red representing higher resistivity (low conductivity).

The interpretation of the modelled apparent resistivity sections is based on published electrical properties of typical sub-surface materials outlined in Section 1.3.3.

The measured resistivity values range from ~0 Ωm to ~2500 Ωm. This range of values indicates a relatively broad distribution of clay-rich and clay-deficient materials. Typically, values < 100 Ωm indicate an increasing influence of clay and/or moisture. Higher values are considered relatively clay or moisture-deficient and indicative of more granular materials. The ERT surveys have characterised the dam structure into two main geoelectrical units:

Unit 1 (green and blue, < 90 Ωm): Shallow, low resistivity values which thin down the embankment. This delineates material with high clay content close to the dam crest and is thought to represent the engineered fines which abut the dam core. Further away from the crest, this material is likely to indicate the superficial Diamicton (glacial till/boulder clay) and shallow engineered 'peat.' As previously discussed, the 'peat' is thought more likely to be composed of mixed materials including peat, silts gravels and clay, given its use as an engineered material. Due to the geo-electrically non-unique nature of these two materials, it is not possible to differentiate between the engineered material ('peat') and the Diamicton using ERT alone.

Unit 2 (yellow and red, 90 Ωm to 400 Ωm): Increased resistivity values that extend to depth. These are thought to indicate the bedrock geology (coal measures). The resistivity values can be quite heterogeneous across the survey area, due to variations in the clay content between the interbedded mudstones, coal fragments, and seat-earth/sandstone noted in the borehole. The heterogeneity will be more pronounced on ERT profiles perpendicular to the strike of the geology i.e., ERT lines 4 and 5. More localised changes in resistivity may be caused by variation in the moisture content.

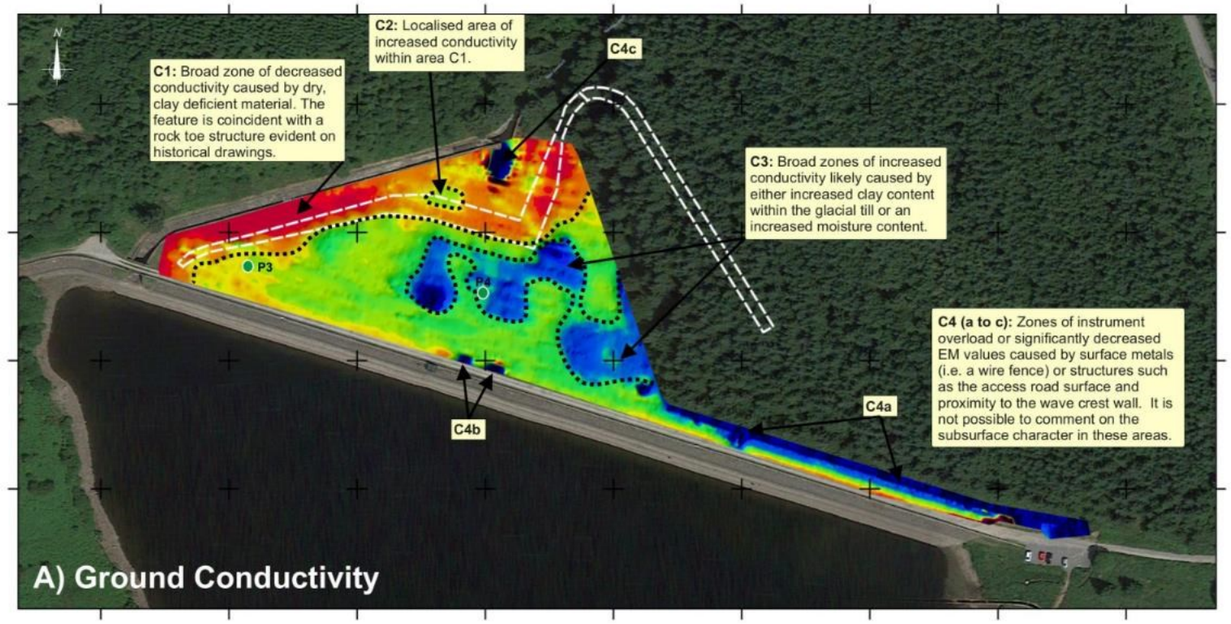

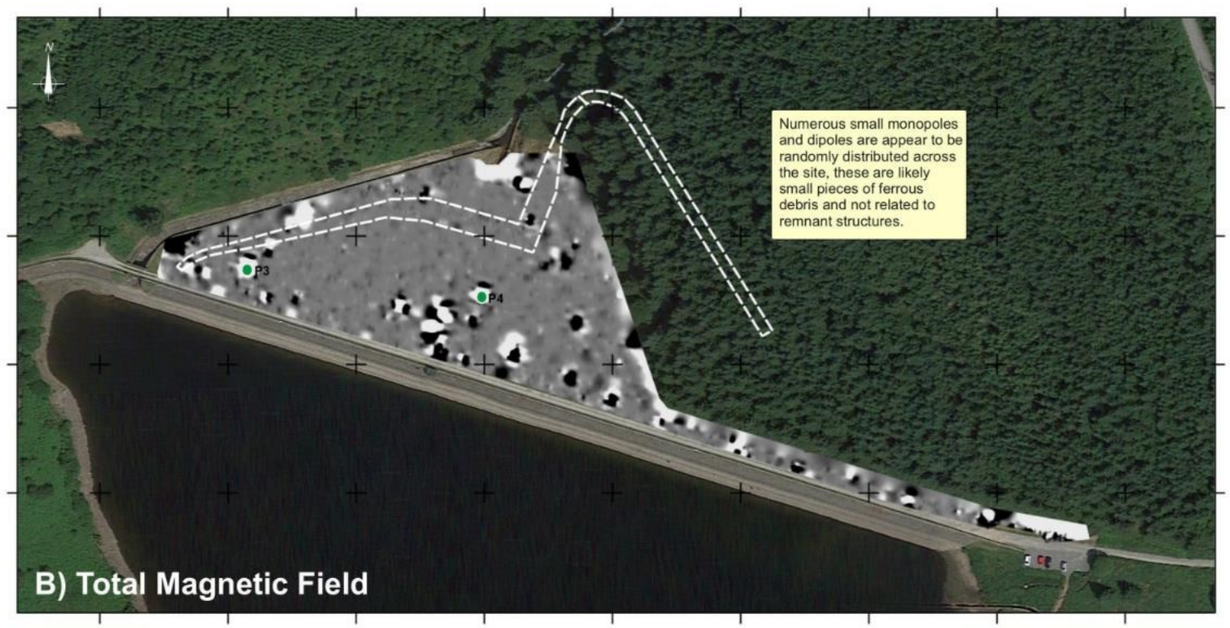

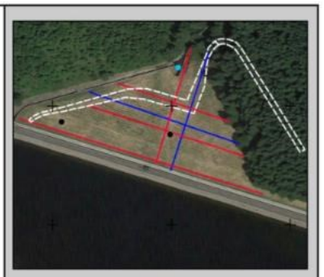

COLOUR SCALES

Conductivity (mS/m)

-18.8 -4.1 -0.7 1.8 3.6 5.3 8.7 8.2 9.8 11.3 13.3 15.8 18.4 21.8 29.8

Magnetic gradient (nT)

-19 -17 -14 -12 -9 -8 -6 -4 -2 0 1 3 4 5 8 8 9 10 13 15 18

SCALES

1 to 2000

25 0 25 50 75

metres

KEY

- Feature boundaries
- Extent of rock toe
- Piezometer locations

NOTES

The fieldwork was completed on the 29th June 2022.

kess dwyrain east

Swansea University Prifysgol Abertawe

Title:

Ground Conductivity and Magnetic Results

Project:

Richard Cottrell MSC by Research

Date:

25th May 2022

FIGURE 5.1

5.3.1 ERT 1

ERT 1 is positioned ~ 3 m downstream of the dam crest, parallel to the dam core. Units 1 and 2 are well defined by the profile; however shallow, high resistivity values dominate the section between 0 m and 45 m chainage, this is likely granular material related to the rubble-stone toe and construction of the spillway. Given the proximity to the dam core, it is likely that Unit 1 is largely comprised of the 'engineered fines' which abut the puddle clay core. Zones of decreased resistivity within Unit 1 suggest a localised increase in moisture or clay content such as features R1 and R2.

5.3.2 ERT 2

ERT 2 is positioned ~ 30 m down the embankment, parallel to the core. Unit 1 is characterised by low resistivity values, which extend to a depth of ~ 360 mAOD. Unit 1 is thinner here than observed closer to the crest. There are very shallow lenses of highly resistive material at the surface. Unit 2 is more heterogeneous than observed along ERT 1, this may be related to variations in clay content due to the interbedded nature of the coal measures.

5.3.3 ERT 3

ERT 3 is located close to the foot of the embankment traversing along the rubble-stone toe, parallel to the dam crest. The profile is dominated by the highly resistive values caused by the granular, dry material of the rubble-stone toe up to a chainage of 70 m, the transition from Unit 1 to Unit 2 is not observable in this area. Unit 1 can be observed between chainage 75 m and 90 m. A subvertical, low resistivity feature R3 is observed at a chainage of 72 m, and this is thought likely to be caused by increased moisture content possibly representing a potential ingress into the dam caused by the existence of the rubble-stone toe. Beneath the rubble-stone toe, the resistivity values are anomalously low where Unit 2 is expected (R4). This could be a subsurface ponding of water within or below the rubble-stone toe or an increase in clay content within the bedrock geology.

5.3.4 ERT 4

ERT 4 is located perpendicular to the dam extending from the crest past the northern toe of the embankment. At the southern end of the profile from 60 m to 100 m chainage Unit 1 can be observed above 360 mAOD. At ~ 55 m chainage, feature R3 (observed on ERT 3) is also visible (a sub-vertical, low resistivity feature extending from the surface). Feature R4 is also observed, potentially extending beneath the rubble-stone toe structure. Unit 2 is identifiable between 0 m and 40 m chainage. However, Unit 1 appears to terminate against the rubble-stone toe structure as suggested by the initial conceptual site model. At the northern foot of the dam, the shallow surface appears to comprise more resistive (clay deficient and/or dry) material.

5.3.5 ERT 5

ERT 5 is located perpendicular to the dam extending from the crest and along the rubble-stone toe, to the east of ERT 4. At the southern end of the profile from 60 m to 100 m chainage Unit 1 can be observed above 355 mAOD. At ~ 58 m chainage, feature R3 is visible. Feature R4 is also observed. The rubble-stone toe is observed as an elongated zone of high resistivity between 0 m and 50 m chainage.

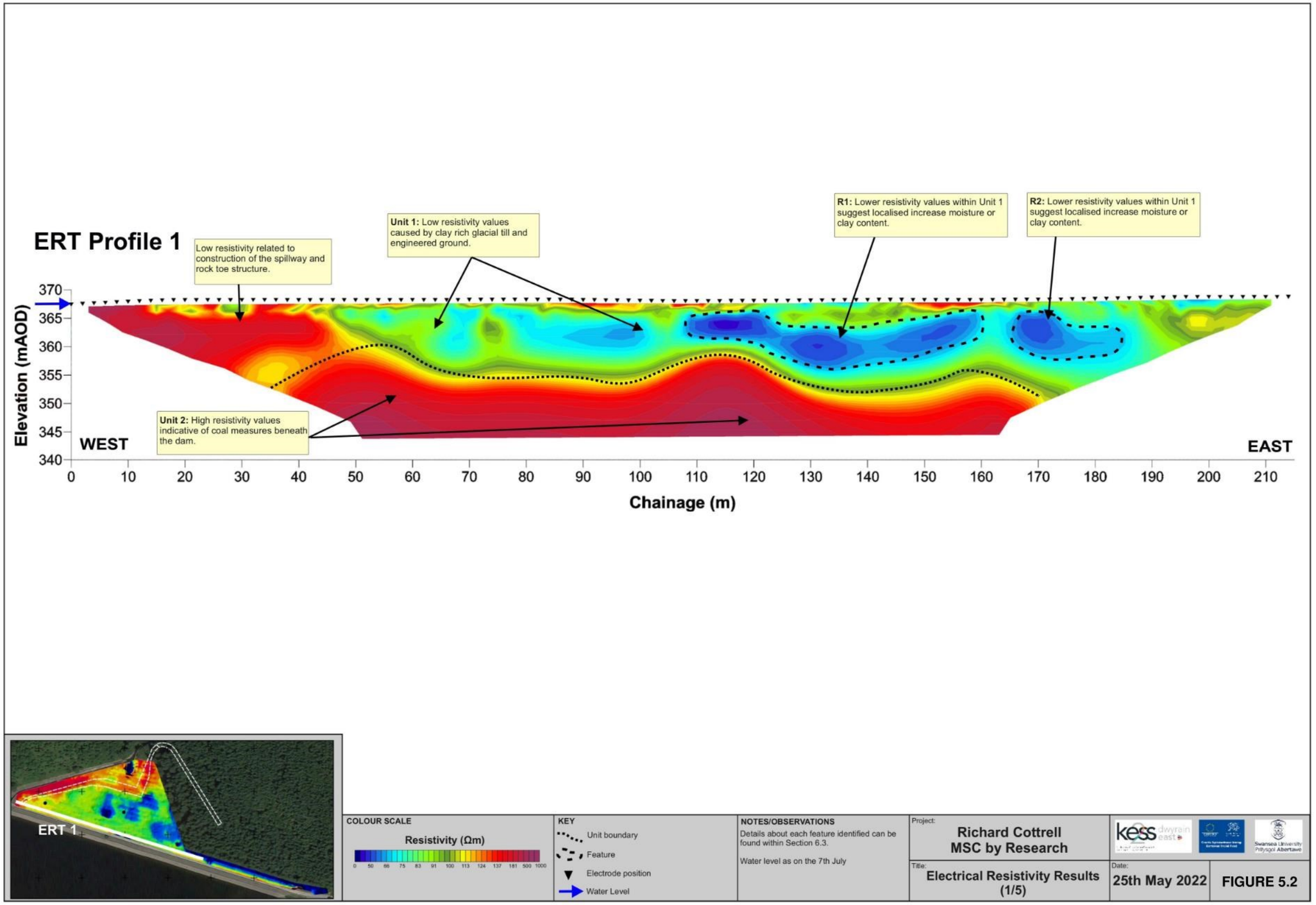
ERT Profile 1
Low resistivity related to construction of the spillway and rock toe structure.
Unit 1: Low resistivity values caused by clay rich glacial till and engineered ground.
R1: Lower resistivity values within Unit 1 suggest localised increase moisture or clay content.
R2: Lower resistivity values within Unit 1 suggest localised increase moisture or clay content.
Unit 2: High resistivity values indicative of coal measures beneath the dam.
WEST
EAST
Elevation (mAOD)
370
365
360
355
350
345
340
0 10 20 30 40 50 60 70 80 90 100 110 120 130 140 150 160 170 180 190 200 210
Chainage (m)
ERT 1
COLOUR SCALE
Resistivity (Ωm)
0 50 66 75 83 91 100 113 124 137 181 500 1000
KEY
Unit boundary
Feature
Electrode position
Water Level
NOTES/OBSERVATIONS
Details about each feature identified can be found within Section 6.3.
Water level as on the 7th July
Project:
Richard Cottrell
MSC by Research
Title:
Electrical Resistivity Results (1/5)
Date:
25th May 2022
FIGURE 5.2

ERT Profile 2

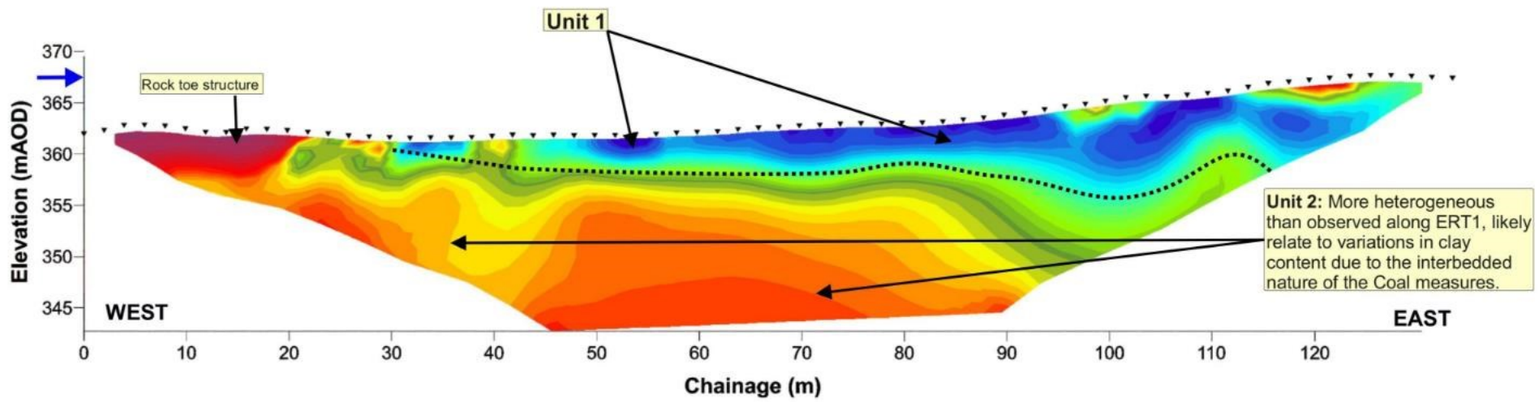

ERT Profile 3

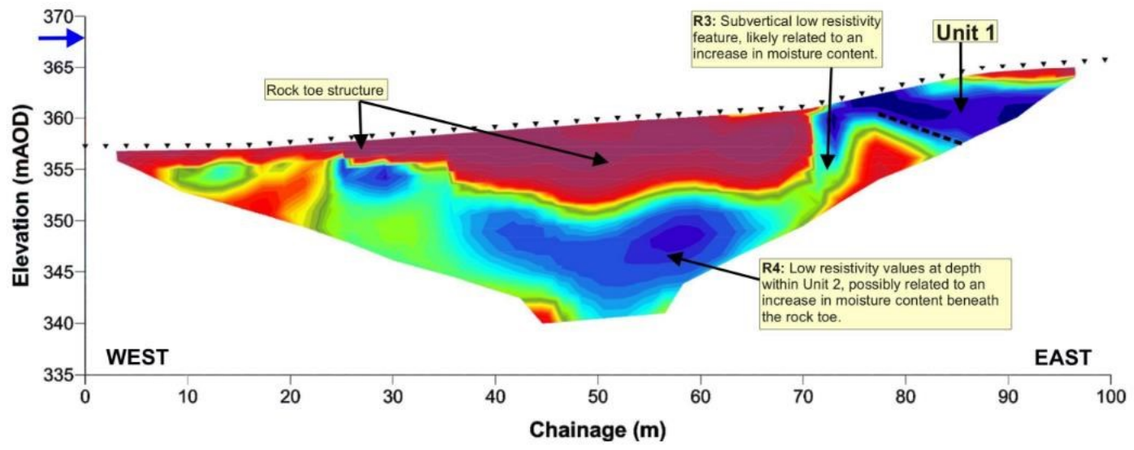

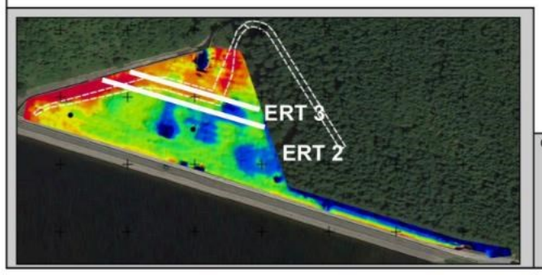

COLOUR SCALE

Resistivity (Ωm)

0 50 66 75 83 91 100 113 124 137 181 500 1000

KEY

Unit boundary

Feature

Electrode position

Water Level

NOTES/OBSERVATIONS

Details about each feature identified can be found within Section 6.3.

Water level as on the 7th July

Project: Richard Cottrell MSC by Research

Title: Electrical Resistivity Results (2/5)

Date: 25th May 2022

FIGURE 5.3

ERT Profile 4

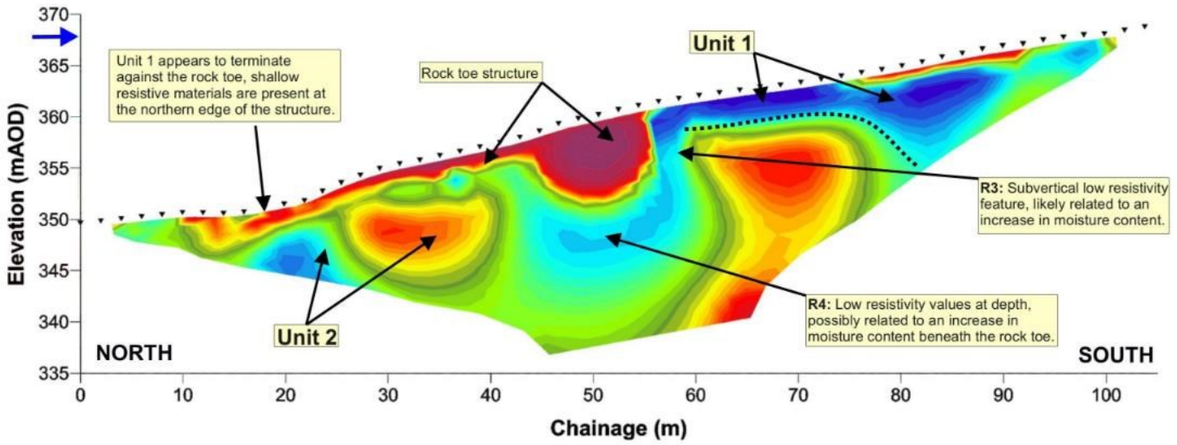

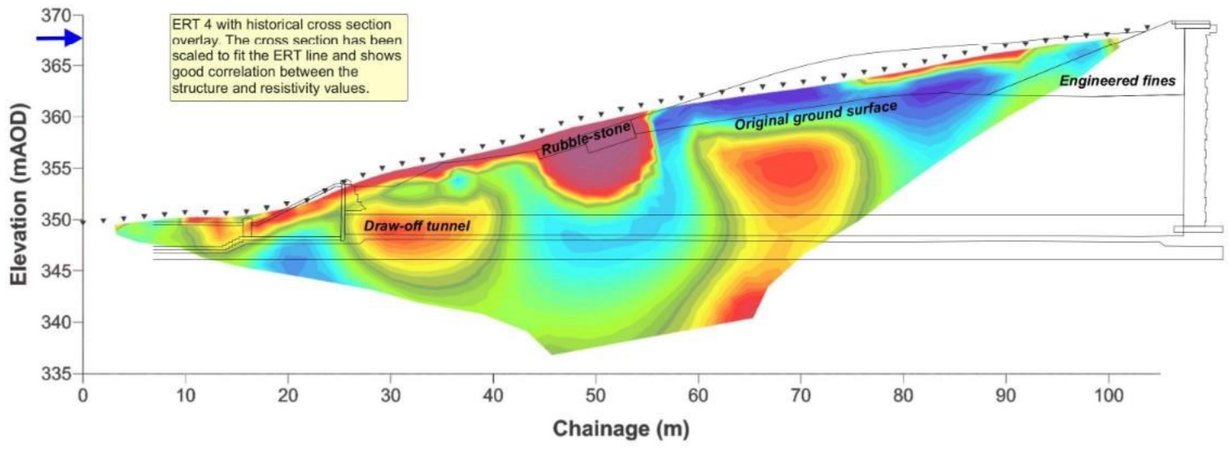

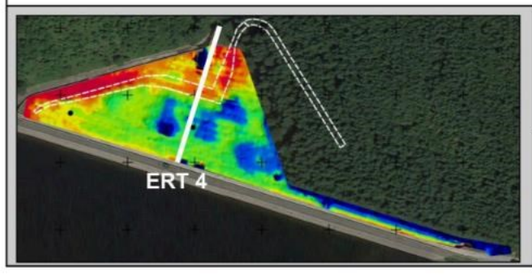

COLOUR SCALE

Resistivity (Ωm)

0 50 66 75 83 91 100 113 124 137 181 500 1000

KEY

- Unit boundary
- Feature
- Electrode position
- Water Level

NOTES/OBSERVATIONS

Details about each feature identified can be found within Section 6.3.

Water level as on the 7th July

Project: Richard Cottrell MSC by Research

Title: Electrical Resistivity Results (3/5)

Date: 25th May 2022

FIGURE 5.4

5.4 Induced Polarisation (IP)

IP data was acquired along ERT 5 to calculate the corresponding normalised chargeability. Calculating normalised chargeability allows for the differentiation between the clay-rich and moisture-rich zones not possible by using ERT alone. Areas of low resistivity and relatively high normalised chargeability are attributed to clay-rich material. Areas of low resistivity and low normalised chargeability are attributed to clay deficient material with high moisture content. The result is displayed on Figure 5.5 on a binary scale showing low normalised chargeability in green and higher normalised chargeability in brown; areas with resistivity values of less than 55 Ωm have been superimposed onto the section shown in blue.

Figure 5.5 shows the calculated normalised chargeability for ERT profile 5, the zone of high normalised chargeability, coincident with particularly low resistivity within Unit 1 (R5), suggests a high clay content and not the presence of moisture downstream of the dam crest. There is no observed increase in normalised chargeability associated with features R3 and R4, suggesting they are caused by an increase in water content within the dam (dominated by bulk conductivity effects, i.e., porewater).

5.5 3D ERT Model

Figure 5.6 presents ERT as a contoured and clipped 3D resistivity model. Ten ERT profiles were used to make this model. The data is cropped at an elevation of 340 mAOD to show variations in the solid geology under the embankment. The 55 Ωm contour was selected for comparison with Figure 5.5. C3 is identified, showing a broad zone of lower resistivity material on the eastern side of the embankment likely caused by either an increase in clay content within the shallow subsurface or an increase in moisture content. Unit 2 is identified as expected, however, it does not extend all the way underneath the dam. R3 is shown as an isolated feature that connects with R4. R3 is represented as a 55 Ωm contour. At higher resistivity contours, this feature can still be observed; however, it is much broader. This suggests a broad increase in moisture content (concluded from IP interpretation), terminating at and passing under the rubble-stone toe that is focused around R3. This suggests that R3 is a preferential surface water infiltration pathway.

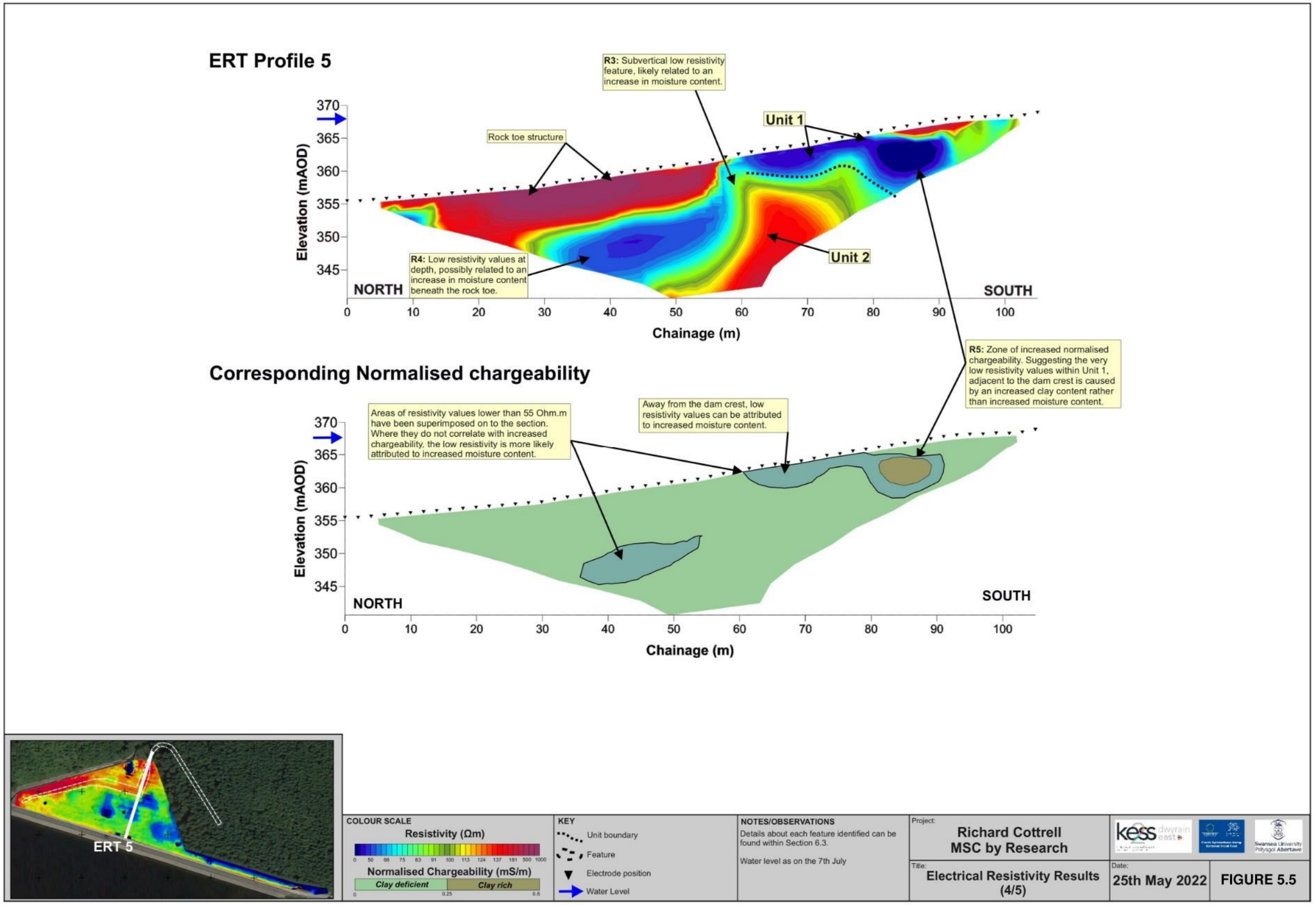
ERT Profile 5
R3: Subvertical low resistivity feature, likely related to an increase in moisture content.
Unit 1
Rock toe structure
Unit 2
R4: Low resistivity values at depth, possibly related to an increase in moisture content beneath the rock toe.
NORTH
SOUTH
Elevation (mAOD)
370
365
360
355
350
345
0
10
20
30
40
50
60
70
80
90
100
Chainage (m)
R5: Zone of increased normalised chargeability. Suggesting the very low resistivity values within Unit 1, adjacent to the dam crest is caused by an increased clay content rather than increased moisture content.
Corresponding Normalised chargeability
Areas of resistivity values lower than 55 Ohm.m have been superimposed on to the section. Where they do not correlate with increased chargeability, the low resistivity is more likely attributed to increased moisture content.
Away from the dam crest, low resistivity values can be attributed to increased moisture content.
NORTH
SOUTH
Elevation (mAOD)
Chainage (m)
ERT 5
COLOUR SCALE
Resistivity (Ωm)
0 50 66 75 83 91 100 113 124 137 181 500 1000
Normalised Chargeability (mS/m)
Clay deficient
Clay rich
0
0.25
0.6
KEY
Unit boundary
Feature
Electrode position
Water Level
NOTES/OBSERVATIONS
Details about each feature identified can be found within Section 6.3.
Water level as on the 7th July
Project:
Richard Cottrell
MSC by Research
Title:
Electrical Resistivity Results (4/5)
Date:
25th May 2022
FIGURE 5.5

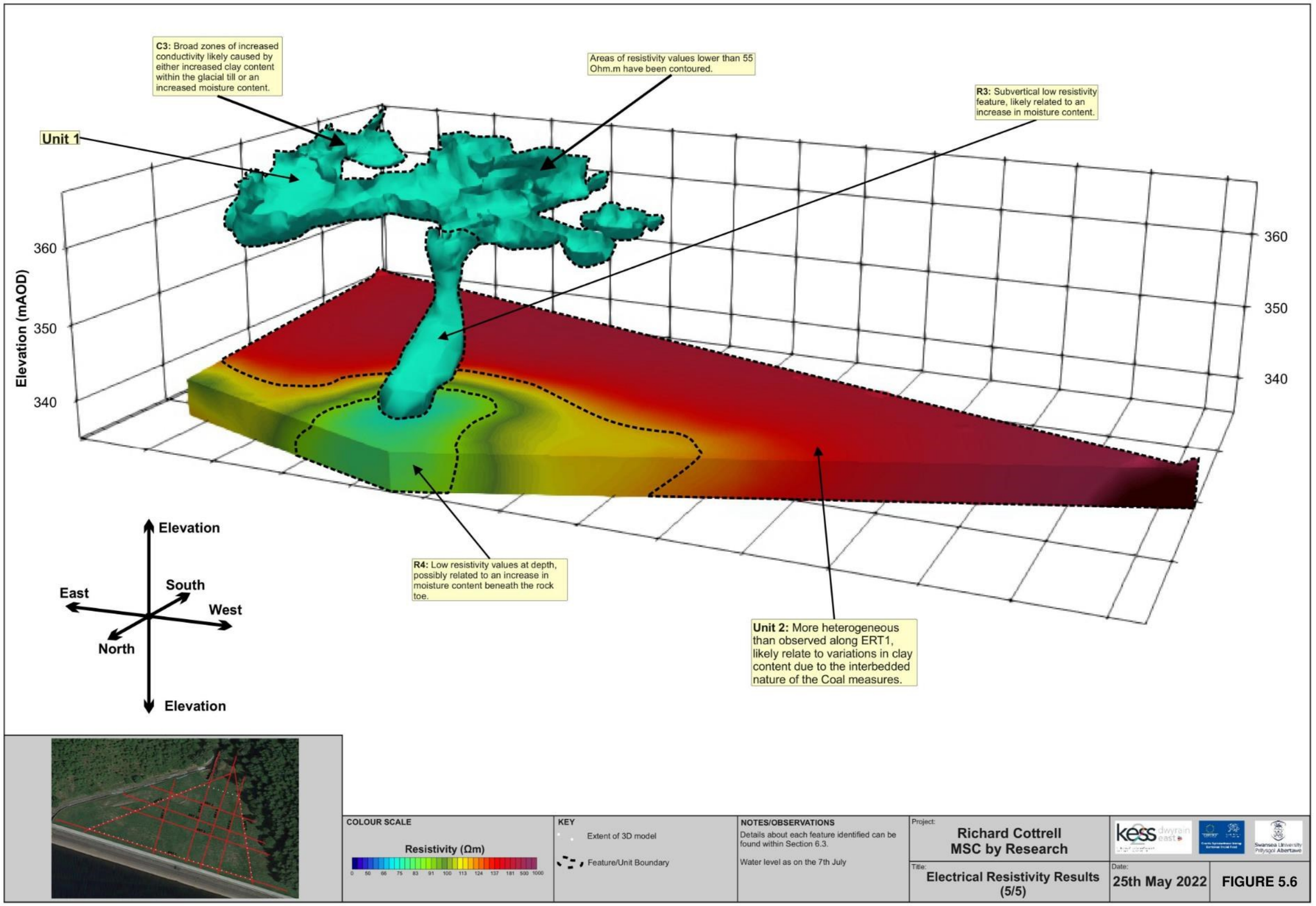
C3: Broad zones of increased conductivity likely caused by either increased clay content within the glacial till or an increased moisture content.
Areas of resistivity values lower than 55 Ohm.m have been contoured.
R3: Subvertical low resistivity feature, likely related to an increase in moisture content.
Unit 1
Elevation (mAOD)
360
350
340
360
350
340
Elevation
East
South
West
North
Elevation
R4: Low resistivity values at depth, possibly related to an increase in moisture content beneath the rock toe.
Unit 2: More heterogeneous than observed along ERT1, likely relate to variations in clay content due to the interbedded nature of the Coal measures.
COLOUR SCALE
Resistivity (Ωm)
0 50 66 75 83 91 100 113 124 137 181 500 1000
KEY
Extent of 3D model
Feature/Unit Boundary
NOTES/OBSERVATIONS
Details about each feature identified can be found within Section 6.3.
Water level as on the 7th July
Project:
Richard Cottrell
MSC by Research
Title:
Electrical Resistivity Results (5/5)
Date:
25th May 2022
FIGURE 5.6

5.6 Self-Potential (SP) Monitoring Network

In December 2022, the results of the SPiVolt monitoring network at the study site were published in the Dams and Reservoirs Journal, created by the Institute of Civil Engineers (ICE). For more information regarding these results, see Hamlyn et al. (2022).

5.6.1 Summary of Self-Potential (SP) Monitoring Results

SP datasets were analysed in conjunction with reservoir level and weather (rainfall) data provided by Dŵr Cymru Welsh Water (except for the period 04/07/2022 – 16/07/2022 where data was acquired from a local weather station). Firstly, the response of SP1 and SP2 was analysed over two periods; when the reservoir level was high (~367 mAOD) and when it was low (~364 mAOD). These periods also coincided with dry weather, negating the effects of rainfall and subsequent surface water flow. SP response during these periods is shown in Figure 5.7. Across the dam's crest, the measured SP became more positive as the reservoir level was lowered. This can be attributed to a general seepage through the dam's core that ceases when the reservoir level is dropped. SP response along the western side of SP1 does not correlate with reservoir level, suggesting that a different mechanism is responsible for SP response in this area. Electrodes in this area are installed on a plateau (see contour shading on Figure 5.7 A). This flat area is therefor able to act as more of a water store than other inclined areas of the embankment. The western edge of SP2 shows a significantly lower SP response than the rest of the profile (F1 on Figure 5.7). This feature is directly downslope of the plateau, suggesting this response is caused by the plateau draining, rather than seepage through the dam's core.

From the characterisation survey, it was hypothesised that seepages into the tunnel at a constant rate are attributed to surface waters higher up the embankment infiltrating the subsurface through the rubble-stone toe and ponding beneath it. This was investigated by looking at the SP response following drying and wetting periods. This was done over a period where the reservoir level was consistently low (post 01/05/2022). The reservoir levels, rainfall data, and corresponding SP responses for different sequences of drying and wetting periods are shown in Figure 5.8. SP data in this instance is presented as a normalised dataset. Normalised negative values (shown in blue) indicate localised areas of increased water flow. Positive normalised values (shown in red) indicate ponding or drying of the subsurface. Electrodes with values of ~ 0 mV suggest no significant response to rainfall. Potential flow pathways are indicated by blue arrows. Table 5.1 summarises each sequence of drying and wetting, the corresponding SP response, and its resulting interpretation.

Table 5.1: *Summary of SP response and interpretation for each drying and wetting sequence.*

Sequence of Wetting and Drying	SP Response	Interpretation
Brief period of rainfall (08/05/2022 – 13/05/2022).	1. East side of the embankment, electrodes downslope of the plateau recorded more negative values. 2. Electrodes along SP 4 show negative values, becoming more positive downslope.	1. Following rainfall, subsurface water moves through this zone (F1). 2. Movement of water downslope as expected, with some ponding beneath the rubble-stone toe.

Wet ground into heat wave (04/07/2022 – 16/07/2022).	1. Across the dam, SP response is generally more positive. 2. Feature F1 becomes narrower.	1. Likely caused by evapotranspiration and 'drying out' rather than ponding water. 2. Feature F1 still remains and active flow path, just narrower.
Dry ground to a month of rainfall (01/05/2022 – 25/05/2022).	1. Positive SP values along SP 4 moved further upslope. 2. Feature F1 becomes wider.	1. Possibly caused by water saturation immediately upslope of the rubble-stone toe. 2. Increased water flow through flow path associated with F1.

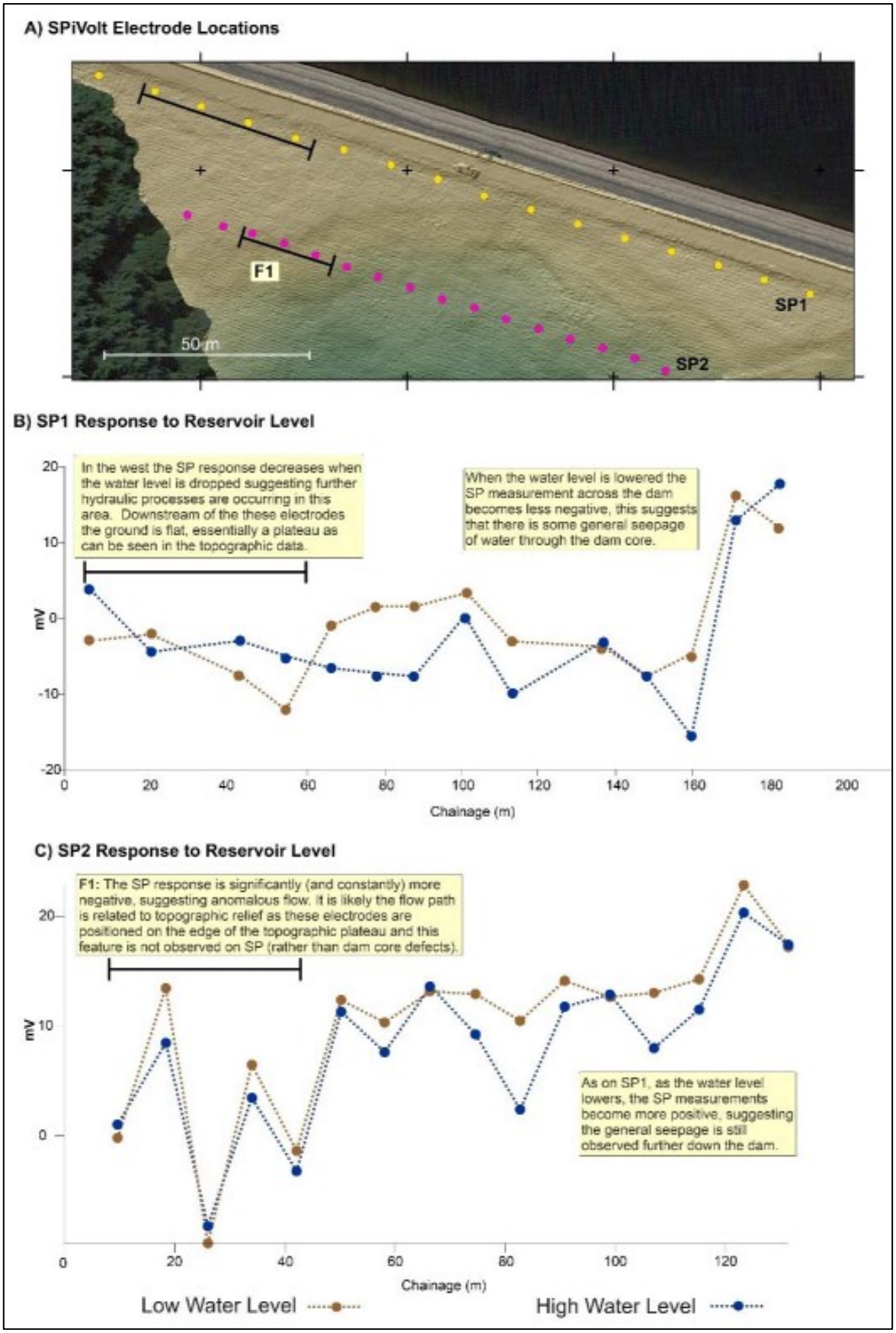

Figure 5.7: A: *Electrode locations of SP1 and SP2 shown in yellow and blue, respectively.* ***B:*** *SP1 response to changing reservoir level.* ***C:*** *SP2 response to changing reservoir level. Taken from Hamlyn et al (2022).*

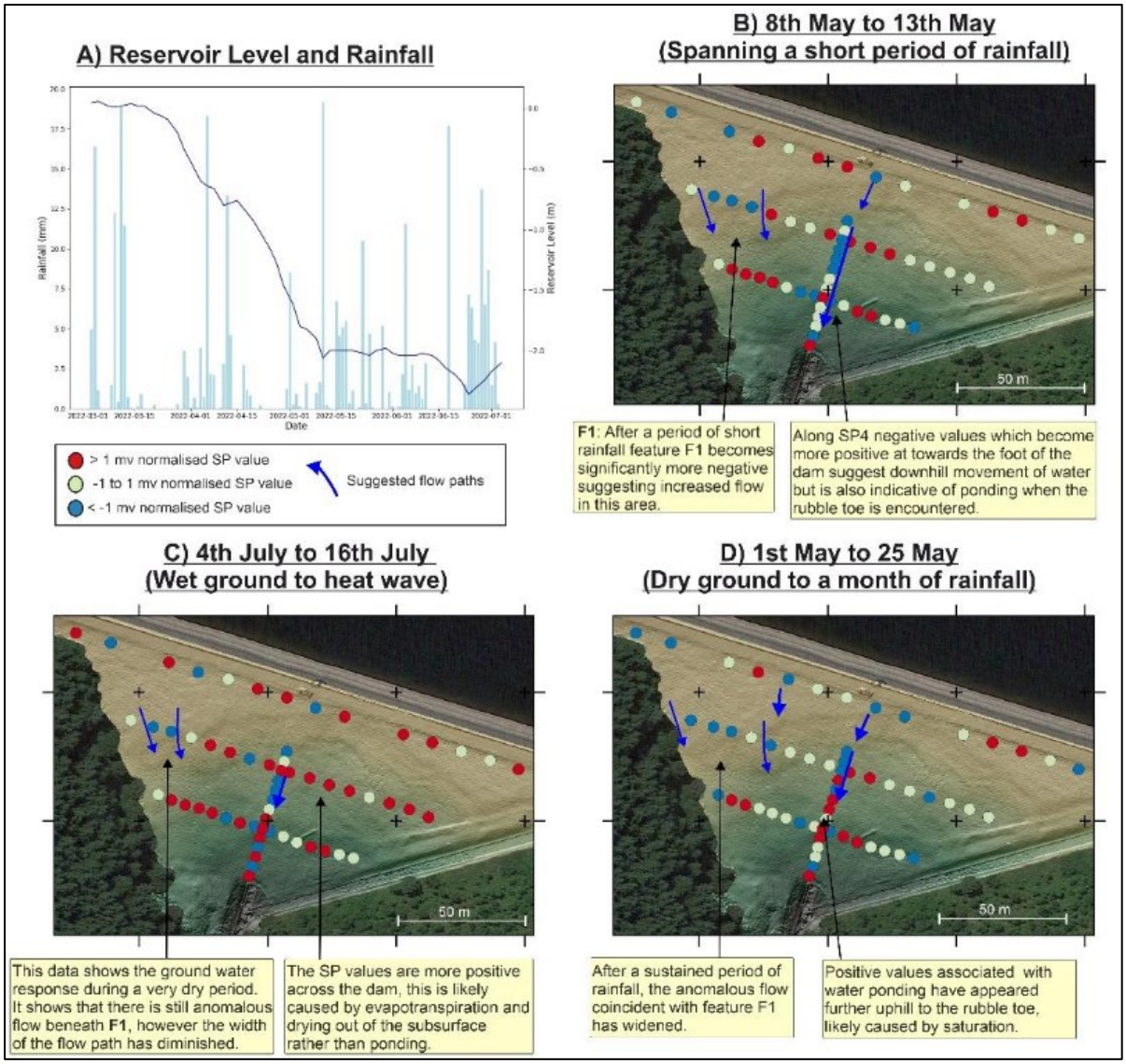

Figure 5.8: ***A:*** *Reservoir level and rainfall data.* ***B-D:*** *Maps of normalised SP response following dry and wet periods. Electrodes which record normalised negative values (shown in blue) indicate localised increased water flow, electrodes that record positive values (shown in red) indicate water ponding or drying of the subsurface, electrodes with values around 0 (+/- 1 mV) suggest no significant localised effects from rainwater. Suggested flow paths are indicated by blue arrows. Taken from Hamlyn et al. (2022).*

6 Discussion

6.1 Conceptual Site Model

The findings of Section 5 are summarised in a revised conceptual site model. This model is presented in Figure 6.1. The model shows how the initial interpretation of the dam's construction materials is representative of the current condition of the site. This includes:

- Two layers (delineated by Unit 1 and Unit 2 in Section 5.3) comprising engineered material/glacial till overlying coal measures.
- The delineation between "engineered fines" towards the crest of the embankment and the thinning out of "peat" downslope.
- The presence of a rubble-stone toe at the toe of the embankment.
- The lack of any unmapped infrastructure/pipework within the downstream shoulder.

In addition to the features confirmed through the characterisation survey, the following was also characterised:

- A potential preferential seepage pathway attributed to surface waters higher up the embankment. These infiltrate the embankment upstream of the rubble-stone toe and pond beneath it.
- A plateau at the top of the eastern side of the embankment which acts as a water store.

Via SP monitoring, the following was confirmed and interpreted:

- Confirmation of the potential seepage pathway identified by the characterisation survey.
- A second preferential seepage pathway through the dam's core, related to the water level within the reservoir.

6.2 Effectiveness of Geophysical Methods

The following sections summarise the relative effectiveness of each characterisation and monitoring technique.

6.2.1 Ground Conductivity

The ground conductivity survey was able to delineate variations in clay and/or moisture content of the downstream shoulder within the top 3 mBGL – 5 mBGL. The data was presented in plan view indicating key features such as the alignment of the rubble-stone toe, and a broad area of increased conductivity located at the eastern side of the embankment. The presence of surface metal at the site limited interpretation in key areas, particularly C4a-c. IP was also considered necessary to delineate between clay rich and moisture rich areas.

This technique was quick and easy to conduct on site and provided a broad overview of the site conditions. These results were used to concentrate ERT and IP survey locations, allowing for greater data density around the key features of interest.

6.2.2 Magnetometry

The magnetometry survey confirmed that there were no additional pipes or utilities beneath the site other than the ones identified by reviewing the historical information. It also confirmed the locations of the piezometers at the site.

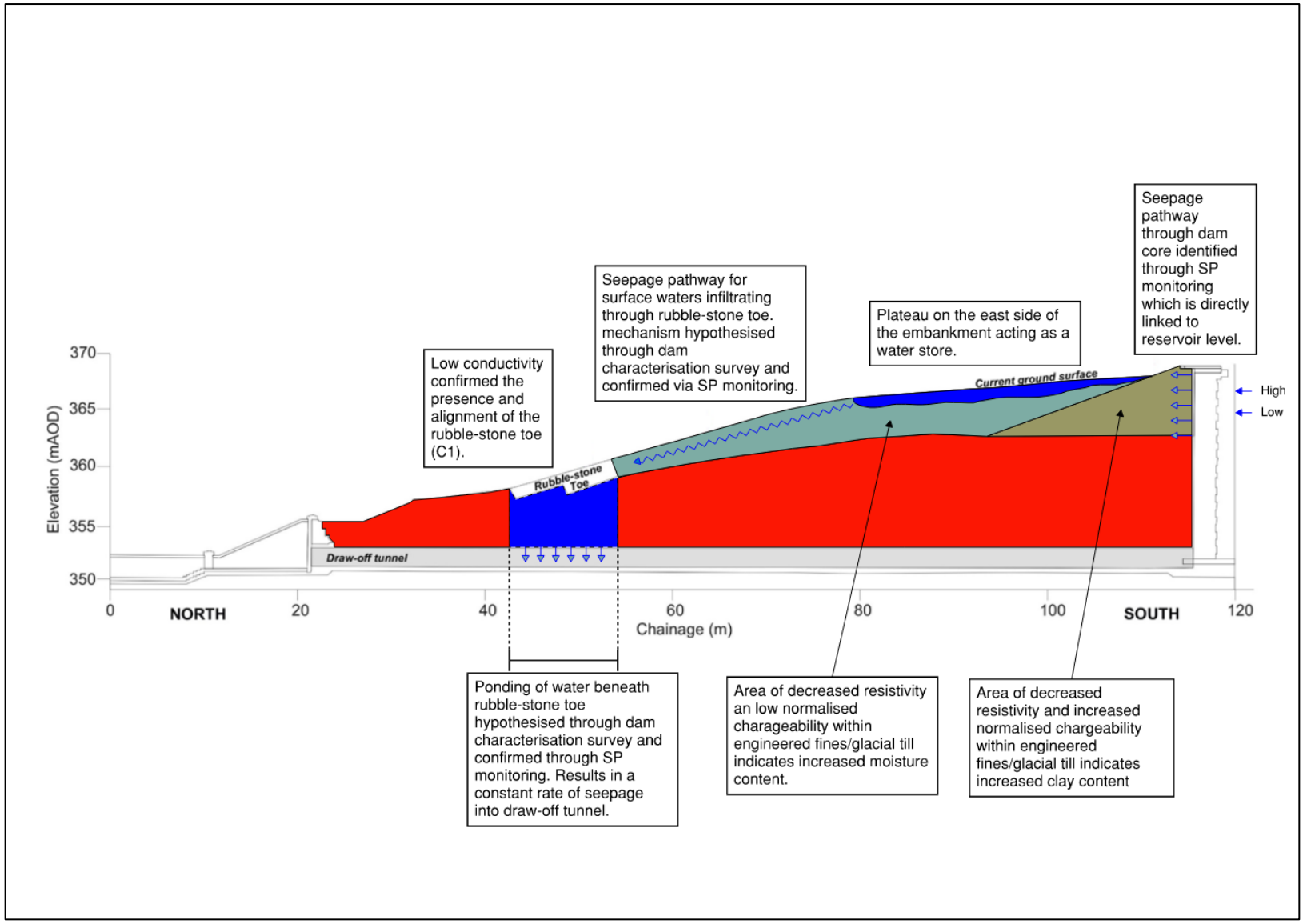

Figure 6.1: *Revised conceptual site model.*

Much like the ground conductivity survey, this technique was easy to conduct and aided the interpretation of the characterisation survey results by removing the potential effects of ferrous materials, thus reducing the impact of non-uniqueness as discussed in Section 1.

6.2.3 Electrical Resistivity Tomography (ERT)

ERT was arguably the most useful characterisation technique deployed at the site. It was able to map the spatial distribution of resistive materials at depth, however, the use of IP was considered necessary to delineate between clay rich and moisture rich zones. Unlike the ground conductivity survey, surface metal has no impact on data quality, therefor, features such as C4c have no influence on the data. This makes this technique ideal for sites where surface metal is common.

Acquiring reciprocal ERT data doubled the time taken to acquire data in the field. Figure 6.2 shows a differential plot of ERT data acquired for ERT 5. The plot shows the difference in modelled resistivity between applying the reciprocal error model and using traditional error statistics (i.e., repeatability) within Res2DInv. Most of the modelled data points did not change within 10 Ωm. The maximum difference were observed at high resistivity values (> 100 Ωm), which is to be expected. The differences in resistivity between the two models did not affect the interpretation of the ERT data. Therefore, it can be concluded that applying this method of ERT error analysis (acquiring one reciprocal data set and applying it to the rest of the ERT data sets) is a commercially valid option. The data does not suggest that acquiring reciprocal measurements for all ERT profiles is commercially viable, i.e., doubling the survey time to acquire this data is not justified in this instance.

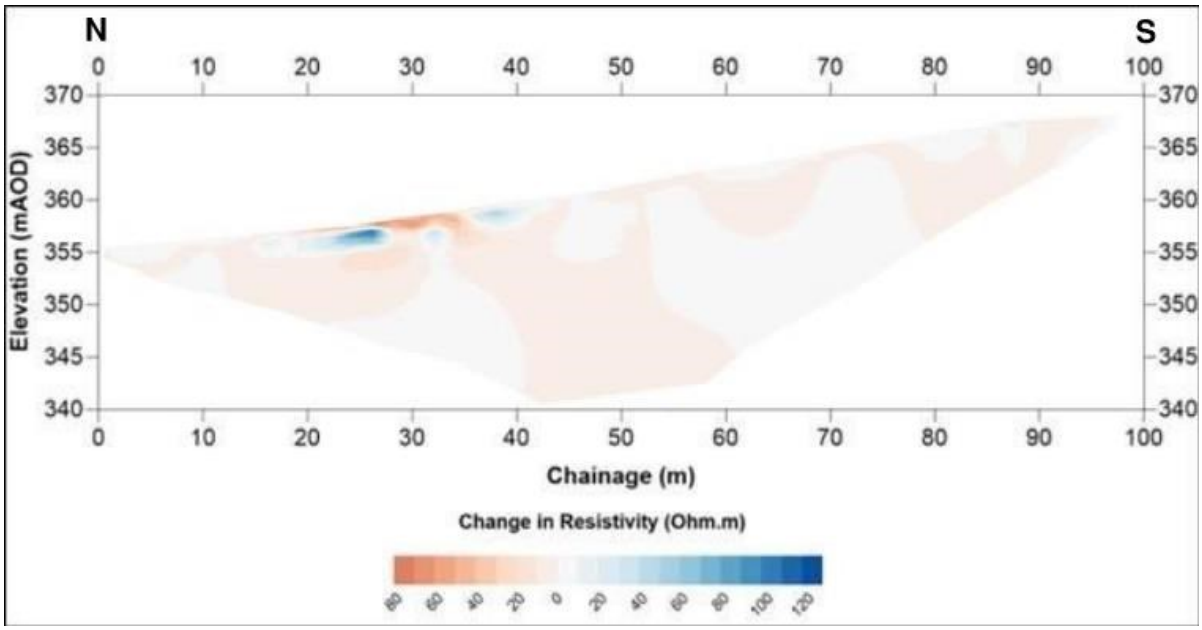

Figure 6.2: *Differential plot of raw data from ERT 5 between* modelled resistivity by applying the reciprocal error model and using traditional error statistics (i.e., repeatability) within Res2DInv.

6.2.4 Induced Polarisation (IP)

Acquisition of IP data allowed clay rich and moisture rich areas to be delineated. This was necessary in forming the hypothesis of a potential preferential seepage pathway attributed to surface waters and ponding beneath the rubble-stone toe. IP was the most effective technique at reducing the impact of non-uniqueness.

6.2.5 3D Modelling of Electrical Resistivity Tomography (ERT) Data

3D inversion of the ERT data was achieved using open-source software. This provided valuable insight in visualising the hypothesised seepage pathway and was a useful tool for facilitating discussions with supervisors and communicating findings with Dŵr Cymru Welsh Water.

6.2.6 Self-Potential (SP) Monitoring

SP monitoring was necessary to confirm the hypothesis proposed by the characterisation survey. Monitoring also identified a second preferential seepage pathway directly related to reservoir level. This was only achievable through monitoring.

It is likely that a general seepage takes place through the dam's core, which ceases when the reservoir is dropped below a certain level between 364 mAOD and 367 mAOD. Historical drawings show the dam's core to comprise "puddle clay." However, the core is more likely to comprise the most clay-rich material that could be found within the immediate vicinity of the dam at the time of construction, not engineered material of a given specification as is standard practice now. It is probable that some amount of seepage takes place through the dam's core, attributed to more granular material. It is this that is responsible for the SP response associated with reservoir level.

6.3 Implications

According to the Section 10 Report conducted under the Reservoirs Act 1975 in March 2011, several seepages were observed at the western side of the rock toe, to the right of the spillway and into the tunnel. It was reported that the seepage by the spillway appears to correlate with rainfall suggesting it is simply surface runoff caused by a blocked French drain. Seepages into the tunnel appeared to be more consistent suggesting an alternate path. Both hypotheses were confirmed through geophysical characterisation and monitoring.

After discussions with Dŵr Cymru Welsh Water in March 2023, they are utilising this information, and further monitoring, to design a targeted grouting campaign and the installation of directed surface drainage at the eastern section of the downstream shoulder.

6.4 Limitations

The limitations of this project that could have been avoided with early intervention were:

- ERT data was only acquired using a Wenner-Schlumberger arrangement. By also utilising a dipole-dipole electrode configuration, R3 would have been imaged in greater detail.

- The 3D ERT model was created from pseudo 3D profiles. Although coverage over the embankment was good, some areas have a greater density of data points than others. It would have been more useful to acquire a true 3D ERT dataset through a grid layout of electrodes. 2D pseudo sections could have then been extrapolated from this.

- IP data was only acquired along one profile. If IP data were acquired across all ERT profiles, sections could have been compared and a 3D model created (like the 3D resistivity model, but instead for normalised chargeability).

- The IP survey was conducted with stainless steel electrodes. It is recommended that non-polarising electrodes (such as porous Cu-$CuSO_4$ pots) are used for IP surveys.

However, some studies have shown that stainless steel electrodes may be a valid option. Often, stainless steel electrodes outperform Cu-$CuSO_4$, and graphite electrodes. This contrary to traditional expectations was first demonstrated in Dahlin et al. (2002). Zarif et al. (2017) explains how Cu-$CuSO_4$ pots sometimes yield poorer results relative to stainless steel electrodes. This is attributed to Cu-$CuSO_4$ pots having a higher contact resistance than stainless-steel electrodes.

- Multiple ground conductivity surveys could have been conducted to identify temporal variations in ground conductivity. This would help characterise the temporal nature of C3.

Limitations that were unavoidable included:

- Ecological constraints on the site meant that the installation of the SPiVolt array was postponed until March 2022. This left little time for the analysis of the SP monitoring data at the time of writing this thesis.

- Due to the limited availability of field assistants, ERT data was acquired over three site visits over the course of one month. Variations in ground conditions may have impacted the resistivity values of profiles taken on different days. To avoid this, it would have been better to acquire all the data on the same day or within one day of each other. It would have also been better to acquire reciprocal data for all the profiles, however, this would have had minimal effect on the interpretation of ERT data as explained in Section 6.2.3.

6.5 Further Research

The next step for this research project would be to image the preferential seepage pathways using SP Tomography. Whilst it is possible to construct current density cross-sections in packages such as Zond SP2D by inverting SP and ERT datasets together, additional information such as the conductivity of the porewater and the zeta-potential of the soil is required to calculate seepage velocities. The SP Tomography method is best explained in Bolève et al. (2009). SP Tomography involves the inversion of SP and ERT datasets, along with additional information, to estimate seepage velocities within one order of magnitude. Figure 6.3 illustrates the process of combining SP and ERT datasets to achieve this.

To apply this to a monitoring case, it would need to be assumed that the resistivity distribution is unchanged with increased moisture content (which is known not to be the case). This could be avoided by combining the SPiVolt system with an ERT monitoring system, such as BGS Prime. However, this would be extremely expensive. Another approach could be to acquire ERT profiles during the summer (after a prolonged period of rainfall) and a low reservoir level; and in winter (during or just after a period of sustained rainfall) and a high reservoir level. This would provide baseline resistivity distributions of the most extreme cases and intermediate distributions could be interpolated from these, assuming a linear change in resistivity distribution.

Besides allowing for more accurate SP Tomography results, repeating ERT profiles (especially ERT 1) at different reservoir levels may give an indication of the horizon and chainage of the preferential seepage pathway through the dam's core. Areas of decreased resistivity would be assumed to be attributed to water entering the downstream shoulder through the core.

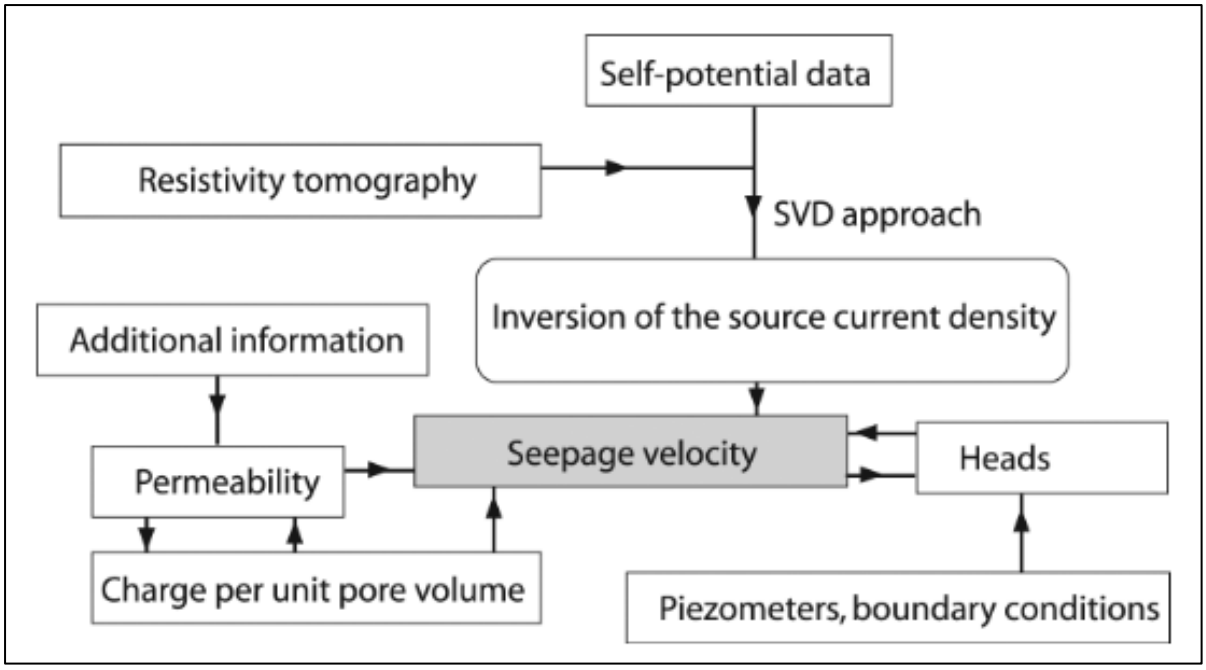

Figure 6.3: *Process to obtain seepage velocities from SP Tomography taken from Bolève et al. (2009).*

7 Conclusions

7.1 Dam Characterisation

- A traditional TerraDat UK Ltd. multidisciplinary geophysical survey was conducted to characterise the ground conditions of the downstream shoulder. The survey comprised ground conductivity, magnetic, and Electrical Resistivity Tomography (ERT) techniques. The ground conductivity and ERT surveys delineated both shallow and deep zones of increased clay and moisture content which correlate well with the known structure of the dam and the surrounding mapped geology. The magnetic survey identified numerous small monopoles and dipoles randomly distributed across the site. However, these are attributed to small ferrous debris and not related to remnant structures. ERT 4 and ERT 5 showed a potential ingress pathway extending from the surface to depth to the south of the rubble-stone toe structure.

- The ERT data in conjunction with normalised chargeability, allowed for the delineation of clay-rich and moisture-rich zones. Interpreting these datasets suggested moisture 'ponding' beneath the rubble-stone toe structure.

- All ten ERT profiles were successfully inverted to produce a 3D resistivity model. The sub-vertical feature identified by ERT 3, 4 and 5 is clear to see in 3D, as well as the areas of relatively increased conductivity identified by the ground conductivity survey and the more heterogeneous nature of the resistivity values at depth attributed to the coal measures. A localised area of decreased resistivity was observed, which is attributed to the ponding water underneath the rubble-stone toe.

- A hypothesis was developed that the deeper tunnel seepage was attributed to surface waters higher up the embankment infiltrating upstream of the rubble-stone toe; and ponding beneath it.

7.2 Self-Potential (SP) Monitoring

- A continuous cable network was developed with the ability to produce accurate, reliable measurements and link with the existing SPiVolt Hub.

- An effective solution for installing SP monitoring arrays was developed making it a practical method to deploy on comparable sites in the future.

- SP monitoring directly mapped subsurface flow through the dam and observed changes to the flow regime linked to reservoir level and rainfall.

- The monitoring approach highlighted anomalous areas within the subsurface that can only be attributed to groundwater flow.

- SP monitoring confirmed the hypothesis put forward from the dam characterisation survey and identified a second preferential seepage pathway through the dams core which is linked to reservoir level.

References

Abdulsamad, F; Revil, A; Soueid Ahmed, A; Coperey, A; Karaoulis, M; Nicaise, Sylvie; Peyras, Lauent., 2019. Induced polarization tomography applied to the detection and the monitoring of leaks in embankments. Engineering Geology, Volume 254, pp. 89-101.

Ahmad, M. U., 1961. A laboratory study of streaming potentials. Geophysical Prospecting, Volume 12, pp. 49-64.

Barde-Cabusson, S., Finizola, A. & Grobbe, N., 2020. A practical approach for self-potential data acquisition, processing, and. Interpretation, 11, Volume 9.

Binley, A., Ramirez, A. & Daily, W., 1995. Regularised image reconstruction of noisy. Bergen, Norway, pp. 6-8.

Bolève, A; Revil, A; Janod, F; Mattiuzzo, J L; Fry, J J., 2009. Preferential fluid flow pathways in embankment dams imaged by self-potential tomography. Near Surface Geophysics, 7(5), pp. 447-462.

British Dam Society, 2022. British Dam Society. Available at: https://britishdams.org/

Butler, D. K. & Llopis, J. L., 1990. Assessment of Anomalous Seepage Conditions. Geotechnical an Environmental Geophysics, Volume 2, pp. 153-174.

Coal Authority, 2023. The Coal Authority Interactive Map Viewer. Available at: https://mapapps2.bgs.ac.uk/coalauthority/home.html

Comsol, 2022. Comsol. Available at: https://www.comsol.com/

Corwin, R. F. & Hoover, D. B., 1979. The self-potential method in geothermal exploration. Geophysics, Issue 44, pp. 226-245.

Knappett, J., & Craig, R. F. (2012). *Craig's soil mechanics* (8th ed.). CRC Press.

Cui, Y. A. et al., 2017. Dynamic imaging of metallic contamination plume based on self-potential data. Transactions of Nonferrous Metals Society of China, Issue 27(8), pp. 1822-1830.

Dahlin, T., Leroux, V. & Nissen, J., 2002. Measuring techniques in induced polarisation imaging. Journal of, Volume 50, pp. 279-298.

Dahlin, T. & Zhou, B., 2004. A numerical comparison of 2D resistivity imaging with 10. Geophysical Prospecting, 5(5), pp. 379-398.

DEFRA, 2011. DEFRA. Available at: https://assets.publishing.service.gov.uk/government/uploads/system/uploads/attachment_data/file/69403/pb13530-waste-hierarchy-guidance.pdf

Drahor, M. G., 2004. Application of the self-potential method to archaeological prospection. Archaeological Prospection, Issue 11, pp. 77-105.

Farnham, N., 2021. Next Generation Monitoring of Critical Welsh Infrastructure: Creating a Starting Point for Integrating Remote Monitoring Data. University of South Wales.

Fell, R., Foster, M. & Wan, C. F., 2004. Methods for estimating the probability of failure of embankment dams by internal erosion and piping-piping through the embankment. University of New South Wales.

Foster, M., Fell, R. & Spannagle, M., 2000. The statistics of embankment dam failures and accidents. Canadian Geotechnical Journal, 37(5), pp. 1000-1024.

Fox, R. W. & Davies, G., 1830. On the electro-magnetic properties of metalliferous veins in the mines of Cornwall. Phil. Trans. R., Issue 120, pp. 399-414.

George, A., 2006. Development of Geoelectric Techniques for Investigation and Monitoring of Landfills. Cardiff University.

Grow, L. L., 1982. Induced polarization for geological exploration. Geophysics: The Leading Edge of Exploration, 1(1), pp. 55-56; 69-70.

Guillaume Blanchy, S. S. J. B. P. M. A. B., 2020. ResIPy, an intuitive open source software for complex geoelectrical inversion. Computers & Geosciences, Volume 137.

Hamlyn, J., Cottrell, R., Bird, C. & Kulessa, B., 2022. Observing waterflow within an embankment dam using self-potential monitoring. Dams and Reservoirs, 33(1), pp. 19-26.

Kayode, O. T., Odukoya, A. M., Adagunodo, T. A. & Adeniji, A. A., 2018. Monitoring of seepages around dams using geophysical. IOP Conf. Ser.: Earth Environ. Sci.

Knappett, J. & Craig, R. F., 2019. Craig's Soil Mechanics. 9th ed. London: CRC Press.

Kulessa, B., Kalin, R., Doherty, R. & Phillips, D., 2006. Self-potential (SP) and active electrical geophysical assessment of bioremediation at a contaminated gasworks plant. In AGU Spring Meeting Abstracts, Volume 2007, pp. NS34A-04.

LaBrecque, D J., Mletto, M., Daily, W., Ramirez, A L. & Owen, E.,1996. The effects of noise on Ocam's inversion of resistivity tomography data. Geophysics, Issue 61, pp. 538-548.

Lénat, J. F., 2007. Retrieving self-potential anomalies in a complex volcanic environment: and SP/elevation gradient approach. Near Surface Geophysics, Issue 5, pp. 161-170.

Milson, J. & Eriksen, A., 2011. Field Geophysics. Fourth Edition ed. Oxford: John Wiley & Sons Ltd.

Mwakanyamale, K., Slater, L., Binley, A. & Ntarlagiannis, D., 2012. Lithologic imaging using complex conductivity: Lessons learned from the Hanford 300 Area. Geophysics, 77(6), pp. 397-409.

Ogilvy, A. A., Ayed, M. A. & Bogoslovsky, V. A., 1969. Geophysical studies of water leakage from reservoirs. Geophysical Prospecting, Issue 22, pp. 36-62.

Panthulu, T. V., Krishnasiah, C. & Shirke, J. M., 2001. Detection of seepage paths in earth dams using self-potential and electrical resistivity methods. Engineering Geology, 59(3-4), pp. 281-295.
ParaView, 2022. ParaView. Available at: https://www.paraview.org/

Patella, D., 1997. Introduction to ground surface self-potential tomography. Geophysical Prospecting, Issue 45, pp. 653-681.

Petiau, G., 2000. Second Generation of Lead-lead Chloride Electrodes for. Pure Applied Geophysics, Volume 157, pp. 357-382.

Prasad, R. & Dixit, M., 2019. Instrumentation And Monitoring of Dams And. International Journal of Engineering and Applied Sciences (IJEAS), 6(10), pp. 1-8.

Revil, A. & Jardani, A., 2013. The Self-Potential Method Theory and Applications in Environmental Geosciences. 1 ed. Cambridge University Press.

Revil, A., Kessouri, M. & Torres-Verdin, C., 2014. Electrical conductivity, induced polarization, and permeability of the Fontainebleau sandstone. Geophysics, 79(5), pp. 301-308.
Revil, A. & Leroy, P., 2001. Hydroelectric coupling in a clayey material. Geophysical Research Letters, 28(8), pp. 1673-1646.

Revil, A. et al., 2007. Electrokinetic coupling in unsaturated porous media. Journal of colloid and interface science, 313(1), pp. 315-327.

Revil, A., Naudet, V., Nouzaret, J. & Pessel, M., 2002. Principles of electrography applied to self-potential electrokinetic sources and hydrogeological applications. Water Resources Research, Issue 39, p. 1114.

Reynolds, J. M., 2011. An Introduction to Applied and Environmental Geophysics. 2nd Edition ed. Chichester: John Wiley & Sons, Ltd.

Richards, K. S. & Reddy, K. R., 2007. Critical appraisal of piping phenomena in earth dams. Bulletin of Engineering Geology and the Environment, 66(4), pp. 381-402.

Rozycki, A., Fonticiella, J. M. R. & Cuadra, A., 2006. Detection and evaluation of horizontal fractures in Earth dams using self-potential method. Engineering Geology, 82(3), pp. 145-153.
Schlumberger, C. & Schlumberger, M., 1922. Electrical Phenomena Produced by Metallic Ores. Comptes Rendus.

Scott, J. B. T., 2006. The origin of the observed low-frequency electrical polarization in sandstones. Geophysics, Volume 71, pp. G235-G238.

SEG, 2022. SEG Library. Available at: https://library.seg.org/

Sentenac, P., Benes, V. & Keenan, H., 2018. Reservoir assessment using non invasive geophysical techniques. Environmental Earth Sciences, Volume 77.

Sheffer, M. R. & Howie, J. A., 2003. A numerical modelling procedure for the study of the streaming potential phenomenon in embankment dams. San Antonio, Texas, USA, pp. 475-487.

Sheffer, M. R. & Howie, J. A., 2001. Imaging subsurface seepage conditions through the modelling of streaming potential. Calgary, pp. 1094-1101.

Slater, L. D. & Lesmes, D., 2002. IP interpretation in environmental investigations. Geophysics, 67(1), pp. 77-88.

Stern, O., 1924. ZUR THEORIE DER ELEKTROLYTISCHEN DOPPELSCHICHT. Zeitschrift für Elektrochemie und angewandte physikalische Chemie, Volume 30, pp. 508-516.

Taboga, A., 2011. The Development of Integrated High-Resolution Geophysical, Photogrammetric and GPS Surveying Applied to Landslides in the South Wales Coalfield, Cardiff University.

Chak-Hau Michael Tso, Oliver Kuras, Paul B. Wilkinson, Sebastian Uhlemann, Jonathan E. Chambers, Philip I. Meldrum, James Graham, Emma F. Sherlock, Andrew Binley., 2017. Improved characterisation and modelling of measurement errors in electrical resistivity tomography (ERT) surveys. Journal of Applied Geophysics, Volume 146, pp. 103-119.

UK Research and Innovation, 2020. UKRI. Available at: https://www.ukri.org/

Ulrich, C. & Slater, L., 2004. Induced polarization measurements on unsaturated unconsolidated sands. Geophysics, Volume 69, pp. 762-771.

Varotos, P. & Alexopoulos, K., 1984. Physical properties of the variations of electric field of the earth preceding earthquakes. Tectonophysics, Issue 110, pp. 73-98.

Von Thun, J. L., 1996. Understanding seepage and piping failures – the No. 1 dam safety problem in the west. Kentucky, Association of State Dam Safety Officials.

Wang, M. & Revil, A., 2010. Electrochemical charge of silica surface at high ionic strength in narrow channels. Journal of Colloid and Interface Science, Issue 343, pp. 381-386.

Wilt, M. J. & Corwin, R. F., 1989. Numerical modelling of self-potential anomalies due to leaky dams: Model and field examples. Berlin, Heidelberg, Springer.

Wynn, J. C. & Sherwood, S. I., 1984. The self-potential (SP) method: an inexpensive reconnaissance and archaeological mapping tool. Journal of Field Archaeology, Issue 11, pp. 195-204.

Zablocki, C. J., 1976. Mapping thermal anomalies on an active volcano by the self-potential method, Kilauea, Hawaii. San Francisco, pp. 1299-1309.

Zairf, F., Kessouri, P. & Slater, L., 2017. Recommendations for field-scale induced polarization (IP) data acquisition and interpretation. Journal of Environmental and Engineering Geophysics, 22(4), pp. 395-410.

Zond, 2022. Zond. Available at: http://zond-geo.com/english/